DRFC/CAD

EUR-CEA-FC-1560

PLASMA DIAGNOSTICS USING SYNCHROTRON RADIATION IN TOKAMAKS

I. Fidone, G. Giruzzi, G. Granata

September 1995

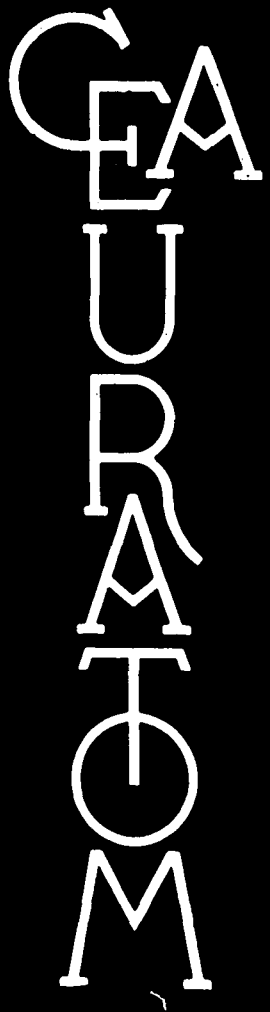

ASSOCIATION EURATOM-C.E.A.
DEPARTEMENT DE RECHERCHES
SUR LA FUSION CONTROLEE
C.E.N./CADARACHE
13108 SAINT PAUL LEZ DURANCE CEDEX

PLASMA DIAGNOSTICS USING SYNCHROTRON RADIATION IN TOKAMAKS

I. Fidone*, G. Giruzzi, G. Granata

Association EURATOM-CEA sur la Fusion
Département de Recherches sur la Fusion Contrôlée
Centre d'Etudes de Cadarache
13108 St. Paul-lez-Durance (FRANCE)

Abstract. Emission of synchrotron radiation for plasma diagnostic purposes in existing and next step tokamaks at arbitrary density and temperature is discussed. This new method is motivated by the need to overcome several deficiencies, caused by cut-off, refraction, and harmonic overlap, and to enhance the informative contents of the familiar low harmonic scheme. In fact, the source of the optically thick low harmonic radiation is highly localized in the ordinary space near the resonance points, and it is found that the energy of the emitting electrons lies in the subthermal range. The measured temperature is then that of subthermal electrons and the method gives no information on the actual temperature of thermal and superthermal electrons. High frequency synchrotron radiation is not restricted by density and temperature upper limits, it is somewhat localized in the ordinary space, and is emitted by electrons over a wide spectrum of energies, ranging from thermal to superthermal values. The basic theory of the method is presented and illustrated by numerical applications, for plasma parameters of relevance in present and next step tokamaks. It is shown that the electron temperature in Maxwellian plasmas can be measured from the radiation spectrum in the frequency ranges where the plasma is optically thick and optically thin, without any *ad hoc* assumption on the effective wall reflection coefficient. Non-thermal features due to rf absorption and a dc electric field are also briefly discussed.

PACS numbers : 52.25.Sw, 52.35.Hr, 52.50.Gw

* Permanent address: Via Colombo 149, I-97018 Scicli (RG), Italy.

I. Introduction

As it is known, electron cyclotron emission (ECE) from a magnetized plasma is determined by the electron energy and therefore the emitted frequency spectrum is in principle suited for diagnosis of the electron momentum distribution. In particular, in tokamak plasmas, radiation near the first few harmonics of the electron gyrofrequency ω_c is routinely used for temperature measurements and investigation of non-thermal features on the electron energy distribution. However, low harmonics have several important limitations. Firstly, low harmonic radiation is affected by cut-off, refraction, and harmonic overlap, and will face severe restrictions in next-step tokamaks, operating at high density and temperature. Secondly, emission of radiation at frequency ω near ω_c, $2\omega_c$ is generated by electrons located at the point x_c determined by the relation $\omega = \omega_c(x_c)$, $2\omega_c(x_c)$. This is a great advantage, since the information carried out by the radiation is very localized in the ordinary space. The disadvantage is that the energy of the emitting electrons $E = mc^2(n\omega_c/\omega-1)$ is lower than the thermal energy and no information on the electron distribution above thermal is obtained from the radiation measurements. In view of that, it is worth investigating the informative potential of electron synchrotron emission[1-3] (ESE) at $\omega \gg \omega_c$, which is generaly unaffected by cut-off and refraction. Furthermore, emission at arbitrary frequency $\omega \neq \omega_c$, $2\omega_c$ is somewhat localized[2] in ordinary space, and the emitting electrons are in a wide range of energies, from subthermal to superthermal values, which enhances the informative contents of the emitted radiation.

A significant part of the emitted radiation at arbitrary frequencies $\omega > 2\omega_c$ is optically thin. Information from this part of the spectrum relies on the knowledge of the effective reflection coefficient $R_f(\omega)$. This is defined as a generalization of the ideal plane slab reflection coefficient and takes into account surface irregularities, conversion between ordinary (O) and extraordinary (X) modes at reflection, spurious contribution due to oblique radiation, and so on. In a reactor, this problem will be less severe than in existing devices, because: i) all the interesting part of the ESE spectrum is in the optically thick or gray range, rather than in the optically thin one; ii) the materials used for the first walls are expected to be less reflecting[4]. However, since the

computation of $R_f(\omega)$ from first principles is hopeless, we avoid *ad hoc* assumptions on the value of $R_f(\omega)$ by proceeding as follows. The emitted spectrum generally displays a number of maxima and minima at $\omega = \omega_i^*$. The values of ω_i^* and of the spectrum intensity $I(\omega_i^*)$ depend on the electron momentum distribution and on $R_f(\omega_i^*)$. At $\omega = \omega_i^*$, the two dependencies are related by the equation $dI/d\omega = 0$, and therefore $I(\omega_i^*)$ becomes a function of the electron distribution only. In the optically thin range of frequencies, we restrict our analysis to frequencies in the vicinity of ω_i^* and the arbitrary choice of the value of the reflection coefficient is avoided. This procedure is in principle applicable to optically thin emission at downshifted frequencies $\omega < \omega_c$ and $\omega < 2\omega_c$, in the absence of cut-off and refraction. The basic procedure for electron temperature measurements on next step tokamaks using ESE relies on the specific properties of the emitted spectrum. This is made up by a portion in the moderate range of frequencies (4th - 6th harmonics), where the plasma is optically thick and the intensity is nearly independent of the temperature spatial profile. This part of the radiation spectrum is appropriate for measuring the electron temperature on axis. The remaining part of the spectrum (typically, above the 6th harmonic), which includes the maximum of emission, will be used for determining the spatial temperature profile.

The plan of the paper is the following. In Sec. II, we discuss the limitations of low harmonics for parameters of relevance in next step tokamaks. In Sec. III, we consider the problem of the effective reflection coefficient and we derive the relation between $R_f(\omega_i^*)$ and $I(\omega_i^*)$, for a plasma with an arbitrary electron momentum distribution and propagation at an arbitrary angle with respect to the magnetic field. In Sec. IV, we present the method for temperature measurements in next step tokamaks using the theory developed in Sec. III. In Sec. V, the electron energy selection for arbitrary frequencies and parameters of interest in present-day and next-step tokamaks is discussed. In Sec. VI, we discuss the problem of diagnosing non-thermal electron distributions by the ESE method. The general conclusions are given in Sec. VII.

II. Limitations of ECE at low harmonics

We first discuss the limitations due to cut-off, refraction, and harmonic overlap in hot and dense plasmas. We consider plasma parameters of relevance for next step tokamaks like ITER[5] (International Thermonuclear Experimental Reactor) and assume the following spatial profiles for electron density and temperature:

$$n_e(\psi) = n_{e0}(1 - \psi^{\alpha_n}), \qquad T_e(\psi) = T_{e0}(1 - \psi)^{\alpha_T}.$$

An elliptical equilibrium and a very flat ($\alpha_n = 5$) density profile are assumed. The relation between the normalized magnetic flux ψ and the Cartesian coordinates (x,y) describing the ellipse with axes (a, b = κa) is given by

$$\psi = [x - x_0(\psi)]^2/a^2 + y^2/b^2, \qquad x_0 = d_0(1-\psi),$$

$$\psi = \frac{1}{2d_0^2}\left(2d_0^2 - 2d_0x + a^2 - \left\{\left(2d_0^2 - 2d_0x + a^2\right)^2 - 4d_0^2\left[(x-d_0)^2 + (y/\kappa)^2\right]\right\}^{1/2}\right),$$

where d_0 is the Shafranov shift. For $d_0 = 0$, $\kappa = 1$, $\psi = r^2/a^2$. The magnetic field is $B_t = B_0/(1+x/R_0)$, the minor radius a = 2.8 m, the major radius R_0 = 7.75 m, B_0 = 5.5 T, κ = 1.6, and d_0 = 0.5 m. The wave propagation is evaluated by means of a toroidal ray-tracing code.

Emission at frequency ω near ω_c (O-mode) or $2\omega_c$ (X-mode) is optically thick and the emitted intensity in the mid-plane, normal to B_t, is given by

$$I(\omega) = \frac{\omega^2}{8\pi^3c^2}\int_{-a}^{a} dx\, T_e(x)\, G(\omega,x)$$

where

$$G(\omega,x) = \alpha(\omega,x)\exp[-\phi(\omega,x)], \quad \phi(\omega,x) = \int_{x}^{a} dx'\, \alpha(\omega,x'),$$

and $\alpha(\omega,x)$ is the local absorption coefficient of the mode considered. Shown in Fig. 1(a) is $T_r(f) = (8\pi^3c^2/\omega^2)I(\omega)$ versus $f = \omega/2\pi$, for the O-mode, T_{e0} = 20 keV, α_T = 1, and $n_{e0} = 10^{20}$ m^{-3} (full thin), $n_{e0} = 2 \times 10^{20}$ m^{-3} (dotted). $T_e(x_c)$ versus $f = f_c(x_c)$ is represented by the full thick curve. Note that the structure of the emission spectrum is more complicated than in the familiar low-temperature regimes. Besides the main peak at f ≈ 143 GHz, related to the maximum of T_e, the spectra have secondary maxima at f ≈ 95 GHz and at f ≈ 200 GHz. These

are due to emission (at the 1st and 2nd harmonic, respectively) coming from high energy electrons (E > 200 keV) in the tail of the Maxwellian, that is sufficiently down-shifted to escape the plasma without substantial re-absorption. This effect limits the range of frequencies for which the ECE spectrum yields the temperature profile. Therefore, it appears that the radiation temperature of the fundamental O-mode coincides with the plasma temperature in the range f ≈ 125 - 180 GHz for $n_{e0} = 2 \times 10^{20}$ m^{-3}, and in the range f ≈ 110 - 180 GHz for $n_{e0} = 10^{20}$ m^{-3}. The dotted curve (high density case) goes to zero abruptly at the cut-off frequency $\omega = \omega_p$. Figure 1(b) shows $T_r(f)$ for the same parameters of Fig. 1(a), but $\alpha_T = 3$. We find that T_r and T_e coincide within the same frequency ranges as for $\alpha_T = 1$. However, for $\alpha_T = 3$ the temperature profile is more peaked and a wider portion of the central profile is accessible. The situation changes for higher values of T_{e0}. Shown in Fig. 2 is $T_r(f)$ for $T_{e0} = 25$ keV and $n_{e0} = 10^{20}$ m^{-3}, $\alpha_T = 1$ (full thin), $n_{e0} = 2 \times 10^{20}$ m^{-3}, $\alpha_T = 1$ (dotted thin), and $n_{e0} = 2 \times 10^{20}$ m^{-3}, $\alpha_T = 3$ (dashed thin). The corresponding $T_e(x_c)$ are represented by the full thick curves. Now the frequency range in which $T_r \approx T_e$ is further reduced. We conclude that the use of the fundamental O-mode in the equatorial plane is restricted to both moderate densities and temperatures.

Next, we consider emission along a chord away from the mid plane in a poloidal cross-section. Now the serious threat is refraction. Shown in Fig. 3 are the ray paths for $n_{e0} = 2 \times 10^{20}$ m^{-3}, f = 130 GHz and increasing values of y at the antenna location. All rays are perpendicular to the toroidal magnetic field at the antenna location, but experience strong refraction during the transit in the plasma region. This shows that the fundamental O-mode is not suited for providing information on the electron temperature profile away from the mid-plane.

Cut-off and refraction effects on second harmonic are in general negligible. Conversely, second harmonic emission is strongly affected by harmonic overlap. Shown in Fig. 4 is $T_r(f)$ for the X-mode, $T_{e0} = 15$ keV, $n_{e0} = 10^{20}$ m^{-3}, and $\alpha_T = 1$, for propagation in the mid-plane normal to the magnetic field. $T_r(f)$ coincides with T_e if we ignore higher harmonics (full thick). The inclusion of the third harmonic contribution (dotted) and third and fourth harmonics

contributions (full thin) changes the result, and $T_r(f)$ deviates significantly from T_e in a wide range of frequencies. The situation is, of course, worse at higher temperatures and/or densities. We conclude that for $T_{e0} \geq 15$ keV, second harmonic emission is a very restrictive method of electron temperature diagnostics.

III. The diagnostic method using ESE

Emission of radiation for arbitrary frequency is described by the equation

$$I(\omega) = \frac{\int_{-a}^{a} dx\, \eta(\omega,x) \exp[-\phi(\omega,x)]}{1 - R_f(\omega)\exp[-\Phi(\omega)]} = \frac{V(\omega)}{1 - R_f(\omega)\exp[-\Phi(\omega)]} , \qquad (1)$$

where $\eta(\omega,x)$ is the emission coefficient, and $\Phi(\omega) = \phi(\omega,-a)$. For thermal plasmas, $\eta = (\omega^2/8\pi^3c^2)T_e\alpha$. The concept of effective reflection coefficient $R_f(\omega)$ is defined as follows. The general solution of the radiation transfer equation is given by

$$I(\omega,a) = I_{in}(\omega,-a) + \int_{-a}^{a} dx\, \eta(\omega,x) \exp[-\phi(\omega,x)] ,$$

where $I_{in}(\omega,-a)$ is the intensity at $x = -a$, propagating towards the receiver at $x = a$. $I_{in}(\omega,-a)$ is here to be considered as an extra source of radiation at frequency ω. The relation between $I_{in}(\omega,-a)$ and $I(\omega,a)$ depends on the symmetry and structure of the reflecting surface. In some simple cases, $I_{in}(\omega,-a) = R_w(\omega)I(\omega,a)$, where $R_w(\omega)$ is the usual reflection coefficient of the wall facing the receiving antenna. In general, $I_{in}(\omega,-a)$ has no simple relation with $I(\omega,a)$. In analogy with the simple case, we formally write $I_{in}(\omega,-a) = R_f(\omega)I(\omega,a)$, where $R_f(\omega)$ is partially related to $r(\omega)$, but generally represents an average effect of several multiple reflections. As shown later on, $I(\omega)$ generally has maxima and minima at several frequencies $\omega = \omega_i^*$. Using the condition $dI/d\omega = 0$ and Eq. (1), and assuming that R_f is a slowly varying function of ω, we obtain

$$\frac{dI}{d\omega} = \frac{[1 - R_f\exp(-\Phi)](dV/d\omega) - V(d\phi/d\omega)R_f\exp(-\Phi)}{[1 - R_f\exp(-\Phi)]^2} = 0 ,$$

from which

$$R_f(\omega_i^*)\exp\left[-\Phi(\omega_i^*)\right]=\left[\frac{dV/d\omega}{dV/d\omega+VdΦ/d\omega}\right]_{\omega_i^*} , \qquad (2)$$

and

$$I(\omega_i^*) = \frac{V(\omega_i^*)}{1-\left[\frac{dV/d\omega}{dV/d\omega+VdΦ/d\omega}\right]_{\omega_i^*}} . \qquad (3)$$

Note that, since R_f appears in front of the exponential factor exp(-Φ), the condition that R_f be a slowly varying function of ω can be more precisely written as $|d(\ln R_f)/d\omega| \ll |d\Phi/d\omega|$, which is a mild restriction. Equation (3) shows that at $\omega = \omega_i^*$, $I(\omega_i^*)$ is determined by the electron momentum distribution only. Assuming that the momentum distribution is characterized by N parameters q_j, these can in principle be determined if the number of maxima and minima is large enough to obtain a number of equations greater or equal to N. In the special case in which the reflection coefficient is zero (namely, in the presence of a radiation dump) or in the optically thin range of frequencies, Eq. (2) establishes a relation between the q_j parameters. Furthermore, since R_f is a slowly varying function of ω, Eq. (1) becomes (piecewise, in the different frequency ranges surrounding the different ω_i^*)

$$I(\omega) = \frac{V(\omega)}{1-\left[\frac{(dV/d\omega)\exp(\Phi)}{dV/d\omega+VdΦ/d\omega}\right]_{\omega_i^*}\exp[-\Phi(\omega)]} . \qquad (4)$$

Equation (4) is the basic equation of the high frequency method. Using emission of the X and O modes normal to the magnetic field and away from normal, one obtains a sufficient number of relations to treat several problems of relevance for present-day and next step tokamaks. In practice, Eq. (4) is applicable if the denominator is not too close to zero, otherwise any small error in the evaluation of V(ω) and Φ(ω) would cause a large error in the determination of I(ω). The denominator of Eq. (4) vanishes if both $R_f \to 1$ and $\Phi \to 0$. Now, detailed studies of the average wall reflection coefficients in a tokamak reactor[4] typically yield $R_f < 0.7$. On the other hand, it will be shown later on that at the maximum of the ESE spectrum one has typically Φ >

0.5 (see Fig. 5). This implies that, in the important part of the spectrum, the denominator of Eq. (4) is at least expected to exceed 0.5, which gives a comfortable margin for a safe use of Eq. (4).

Equation (1) is written for propagation in the equatorial plane normal to the magnetic field. It is however applicable to any chord parallel to the mid-plane by changing the limits of integration. For propagation at an angle $\theta(x)$ with respect to the local magnetic field, we obtain a similar form by changing $dx \rightarrow dx/|\sin\theta_0|$, where θ_0 is the value of θ at the antenna location. Since $\eta(x)$ and $\alpha(x)$ are proportional to n_{e0}, Eqs. (1-4) are valid with the substitution $n_{e0} \rightarrow n_{e0}/|\sin\theta_0|$. For propagation away from normal, $\alpha = \alpha(\omega, N_{||}, x)$, $\eta = \eta(\omega, N_{||}, x)$, $R_f = R_f(\omega,\theta_0)$, $N_{||} = N_{||}(x) = \cos\theta(x)$,

$$I(\omega,\theta_0) = \frac{\int_{x_1}^{x_2} dx\, \eta(\omega,N_{||},x)\, \exp[-\phi(\omega,N_{||},x)]}{1 - R_f(\omega,\theta_0)\exp[-\phi(\omega,N_{||},x_1)]} \quad , \quad \phi(\omega,N_{||},x) = \int_{x}^{x_2} dx'\ \alpha(\omega,N_{||},x') \ ,$$

where x_1 and x_2 are the appropriate limits of integration. In general, for propagation along an arbitrary ray path, we write

$$I(\omega) = \frac{\int_{\ell_1}^{\ell_2} d\ell\, \eta(\omega,\ell)\, \exp[-\phi(\omega,\ell)]}{1 - R_f(\omega,\ell_2)\exp[-\phi(\omega,\ell_1)]} \quad , \quad \phi(\omega,\ell) = \int_{\ell}^{\ell_2} d\ell'\, \alpha(\omega,\ell') \ , \qquad (5)$$

the receiving antenna is located at $\ell = \ell_2$, and we drop the $N_{||}$ dependence.

Note that the only assumption made in the derivation of Eq. (4) is the slow variation of $R_f(\omega)$. If this condition is satisfied, the complications of the toroidal geometry and the irregularities of the wall surface (mixing up information carried by rays propagating at different angles, both poloidally and toroidally) do not affect the validity of Eq. (4). For reactor relevant parameters, at the maximum of the ESE spectrum, the product $R_f\exp(-\Phi)$ is typically less than 0.5, which means that the received rays have experienced no more than 3 - 4 reflections. Thus, the effective reflection coefficient R_f will be not very different from the "true" reflection

coefficient of the wall facing the receiving antenna R_w, and therefore slowly varying with frequency.

IV. Temperature measurements in next-step tokamaks using ESE

Electron synchrotron emission has the potential for determining the electron temperature profile on next-step tokamaks, with central electron temperatures in excess of 20 keV. More precisely, the emitted spectra, both in the mid-plane and away from it, give information on the validity of an assumed profile $T_e(\psi) = T_{e0}(1-\psi)^{\alpha_T}$ for all values of x and y. We discuss this problem for ITER relevant parameters, using the method of Sec. III. The expressions of the local absorption coefficients for an arbitrary isotropic distribution and perpendicular propagation are discussed in Appendix A. They are based on the generalization of the dielectric tensor for a Maxwellian plasma, arbitrary $n > 1$, and arbitrary Larmor radius discussed in Ref. 6. Other formulations of the Maxwellian dielectric tensor are discussed elsewhere[7-9]. In the following numerical study, $n_{e0} = 2 \times 10^{20}$ m^{-3}, and $N_{||} = 0$. Shown in Fig. 5 (a,b,c, respectively) are $I_x(\omega)$, $I_o(\omega)$, and $t_{x,o}(\omega) = \exp[-\Phi(\omega)]$, versus ω/ω_{c0}, for propagation in the mid-plane (y=0), $T_{e0} = 20$ and 30 keV, $\alpha_T = 2$, $R_f = 0.8$ (full) and $R_f = 0$ (dotted). After some oscillations at low harmonics, $I(\omega)$ increases monotonically with ω up to a maximum ω^* and decreases for $\omega > \omega^*$. The emitted radiation is optically thick up to a frequency $\omega_b < \omega^*$, where ω_b mainly depends on T_{e0}. The values of ω^* and $I(\omega^*)$ depend on T_{e0}, α_T, and on the effective reflection coefficient R_f. Note that the principal maxima of the ESE spectra typically occur where the optical depth is of the order of 0.5. An interesting property of the optically thick radiation[3] is that, for $\omega \leq \omega_b$, $I_x(\omega)$ is not only independent of n_e and R_f, but nearly independent of α_T too, namely, for $\omega \leq \omega_b$ $I_x(\omega)$ depends on T_{e0} only. This is illustrated in Fig. 6, where $I_x(\omega)$ is presented for $T_{e0} = 25$ keV, $\alpha_T = 1.5$ (full) and 3 (dashed), $R_f = 0$, 0.8, and 1. It appears that for $\omega \leq \omega_b$, $I_x(\omega)$ is independent of α_T and R_f. This portion of the experimental spectrum is then suited for determining T_{e0} using a best fitting procedure. A similar property holds for the O-mode, if T_{e0} is large enough to obtain a wide range of optically thick radiation.

We now show that the radiation source is somewhat localized in the ordinary space. Shown in Fig. 7 is $G_x(\omega,x)$ versus x for T_{e0} = 25 keV, α_T = 2, and ω/ω_{c0} = 4,5,6,7, and 10. The maximum of G_x lies away from the plasma axis for low values of ω, but tends to be localized near x = 0 for $\omega/\omega_{c0} \geq 6$. For different temperature profiles, the position x_m of the maximum moves towards the region where $T_e(x_m)$ is nearly the same. This explains why the optically thick radiation is nearly independent of α_T.

Due to these properties, for the X-mode Eq. (1) can be better cast in the form

$$I(\omega) = \frac{\omega^2}{8\pi^3 c^2} \langle T_e \rangle \frac{1 - \exp[-\Phi(\omega)]}{1 - R_f(\omega)\exp[-\Phi(\omega)]} \quad , \tag{6}$$

where $\langle T_e \rangle$ is an average value of T_e near the maximum of $G(\omega,x)$. The formal definition of $\langle T_e \rangle$ is

$$\langle T_e \rangle = \frac{\int_{-a}^{a} dx\, T_e(x) G(\omega,x)}{1 - \exp[-\Phi(\omega)]} \quad . \tag{7}$$

The average $\langle T_e \rangle$ is the radiation temperature T_{r1} for $R_f = 1$. T_{r1} increases with ω for $\omega < \omega_b$, remains nearly constant for $\omega > \omega_b$, and is nearly independent of α_T for all values of ω. Shown in Fig. 8 is $T_{r1} = \langle T_e \rangle$, for T_{e0} = 25 keV, α_T = 1.5 (full), and 3 (dotted). Since T_{e0} is now considered to be determined from emission at $\omega \leq \omega_b$, the maximum of $I(\omega)$ is then used to determine α_T, following the analysis of Sec. III. Using Eq. (6), and noting that, for $\omega > \omega_b$, $\langle T_e \rangle$ is independent of ω, Eq. (2) becomes

$$R_f(\omega^*) = \left[\frac{\omega \Phi' \exp(-\Phi) + 2[1 - \exp(-\Phi)]}{\omega \Phi' \exp(-\Phi) + 2[1 - \exp(-\Phi)]\exp(-\Phi)} \right]_{\omega_i^*} \quad , \tag{8}$$

where $\Phi' = d\Phi/d\omega$. Inserting Eq. (8) into Eq. (1), we obtain a relation between ω^*, $I(\omega^*)$, and α_T, which allows the determination of α_T from the experimental spectrum. A second method is to use the X and O modes and apply Eq. (3) to the two maxima, in order to determine T_{e0} and α_T. Once T_{e0} and α_T are found for y = 0, the consistency of the vertical with the horizontal temperature profile can be investigated by observing ESE along different horizontal chords. Examples of X-mode emission spectra at different values of y are shown in Fig. 9(a), for T_{e0}

= 25 keV, R_f = 0.8, and α_T = 2. As expected, for increasing values of y, $I_x(\omega)$ tends to become optically thin for lower values of ω/ω_{c0} [see Fig. 9(b)]. For y = 3 m, the emitted spectrum is similar to that observed on present-day tokamaks.

V. Electron energy selection for arbitrary frequencies.

Information on the energy of the emitting electrons is obtained from the direct radiation source function $G(\omega,x) = \alpha(\omega,x)\exp[-\phi(\omega,x)]$. We first consider the case of second harmonic. The absorption coefficient of the X-mode is given by

$$\alpha_x(\omega,x) \cong \frac{\pi\omega\omega_p^2\mu^2}{30c\omega_c^2 K_2(\mu)\exp(\mu)}\left[\left(\frac{2\omega_c}{\omega}\right)^2 - 1\right]^{5/2} \exp\left[-\mu\left(\frac{2\omega_c}{\omega} - 1\right)\right]$$

$$\cong \frac{4\pi^{1/2}\omega\omega_p^2}{15c\omega_c^2}\xi^{5/2}\exp(-\xi) \quad ,$$

where $\xi = \mu(x_c - x)/R_0$, and K_2 is the McDonald function. $G(\omega,\xi)$ is maximum at $\xi = \xi_m$, where

$$\alpha_x(\omega,\xi_m) = \frac{\mu}{R_0}\left(\frac{5}{2\xi_m} - 1\right) \cong \frac{5\mu}{2R_0\xi_m} \quad ,$$

thus

$$\xi_m = \frac{\mu(x_c - x_m)}{R_0} \cong \left(\frac{75\mu c\omega_c^2}{8\pi^{1/2}R_0\omega\omega_p^2}\right)^{2/7} \quad .$$

For typical parameters of TFTR (Test Fusion Tokamak Reactor), i.e., a = 0.87 m, R_0 = 2.7 m, B_0 = 5.5 T, $n_{e0} = 10^{20}$ m^{-3}, T_{e0} = 11 keV, and x_c = 0, we obtain $\xi_m \approx 1/2$. The half-width of G is $\Delta\xi \approx 1/2$. The energy of the emitting electrons at $\xi = \xi_m$ is given by $E(\xi_m) = mc^2(2\omega_c/\omega - 1) \approx \xi_m T_e \approx T_e/2$. The total range of the emitting electrons is then $0 \lesssim E \lesssim T_e$.

Emission near the second harmonic is localized very close to the resonance point $\omega = 2\omega_c$. This is clearly an advantage. The disadvantage is that it yields the temperature of the subthermal electrons and carries no information on the electron temperature at energies $E > T_e$,

and therefore on the average thermal energy per unit volume. Of course, if it is sure that the distribution is Maxwellian, the temperature may be determined in any energy range, but in general it is desirable to enhance the informative contents of the ECE method. In order to show the relevance of this point, we consider second harmonic emission for a slightly non-Maxwellian isotropic distribution. For an arbitrary distribution function f(γ), we obtain (see Appendix A)

$$\eta_x = \left(\frac{2\pi^2}{15}\right)\frac{\omega}{c}N_x\left(\frac{\omega_p}{\omega_c}\right)^2 mc^2\frac{\omega^2}{8\pi^3c^2}\left[\left(\frac{2\omega_c}{\omega}\right)^2-1\right]^{5/2}[f(\gamma)]_{\gamma=2\omega_c/\omega} \quad ,$$

$$\alpha_x = -\left(\frac{2\pi^2}{15}\right)\frac{\omega}{c}N_x\left(\frac{\omega_p}{\omega_c}\right)^2\left[\left(\frac{2\omega_c}{\omega}\right)^2-1\right]^{5/2}\left[\frac{\partial f}{\partial\gamma}\right]_{\gamma=2\omega_c/\omega} \quad ,$$

for the emission and the absorption coefficients, respectively. For f(γ), we assume

$$f(\gamma) = N\left[1+\frac{1}{\alpha}\mu(\gamma-1)\right]\exp(-\mu\gamma) \quad ,$$

where $\alpha(\gamma) \gg 1$, and N is a normalization factor defined as

$$N = \frac{\mu}{4\pi K_2(\mu)(1+3/2\alpha)} \quad .$$

Since the parameter α is large, the deviation with respect to the Maxwellian distribution is small, namely, $(f - f_M)/f_M \ll 1$ in a wide range of energies. The emitted intensity in the absence of wall reflections is written as

$$I_x(\omega) = \int_{-a}^{a} dx\left(\frac{\eta_x}{\alpha_x}\right)\alpha_x \exp[-\phi(\omega,x)] \quad ,$$

where

$$\frac{\eta_x}{\alpha_x} = -mc^2\frac{\omega^2}{8\pi^3c^2}\left[\frac{f}{\partial f/\partial\gamma}\right]_{\gamma=2\omega_c/\omega} = \frac{\omega^2 T_e}{8\pi^3c^2}\left[\frac{\alpha+\mu(\gamma-1)}{\alpha+\mu(\gamma-1)-1}\right]_{\gamma=2\omega_c/\omega} \quad .$$

The corresponding radiation temperature is then

$$T_r(\omega) = \int_{-a}^{a} dx T_e(x)\left[\frac{\alpha+\mu(2\omega_c/\omega-1)}{\alpha+\mu(2\omega_c/\omega-1)-1}\right]\alpha_x \exp[-\phi(\omega,x)] \quad .$$

It appears that the integral is well approximated by computing the factor

$$T_e(x)\left[\frac{\alpha+\mu(2\omega_c/\omega-1)}{\alpha+\mu(2\omega_c/\omega-1)-1}\right]$$

at the location $x = x_m$ where $\alpha_x \exp(-\phi)$ has a sharp maximum, i.e., for $\xi = \xi_m$ given by the equation

$$\frac{5\mu}{2\xi_m R_0} \approx \alpha_x \approx \left(\frac{4\pi^{1/2}}{15}\right)\frac{\omega}{c}N_x\left(\frac{\omega_p}{\omega_c}\right)^2 N\frac{\alpha-1}{\alpha}\exp(-\xi_m)\xi_m^{5/2} \quad .$$

Since $\alpha \gg 1$, the value of ξ_m is very close to its limit for $\alpha \to \infty$; for instance, for typical TFTR parameters (as discussed above), $\xi_m \approx 1/2$, and

$$T_r \approx T_e(x_c)\frac{\alpha+1/2}{\alpha-1/2} \quad .$$

For $\alpha = 3$, $T_r/T_e \approx 1.4$ and $(f - f_M)/f_M \approx 1/6$. The result obtained for T_r is independent of the energy dependence of α, provided α be finite for $\mu(\gamma-1) = \mu(2\omega_c/\omega-1) \approx \mu(x_c-x_m)/R_0 < 1$. If we assume that $\alpha = $ const. for $\mu(\gamma-1) \ll 1$ and $\alpha \to \infty$ for $\mu(\gamma-1) > 1$, the thermal energy per unit volume (which depends on the distribution function at $\mu(\gamma-1) \approx 3/2$) will be practically unchanged from the Maxwellian case, i.e., $\langle E\rangle \approx n_e(3T_e/2)$. In this case, the value of the radiation temperature is significantly different from $2\langle E\rangle/3n_e$. In the opposite case, namely, $\alpha =$ const. for arbitrary values of $\mu(\gamma-1)$, we obtain

$$\langle E\rangle = n_e\left(\frac{3}{2}T_e\right)\frac{1+5/2\alpha}{1+3/2\alpha} \quad .$$

For $\alpha = 3$, $2\langle E\rangle/3n_e \approx 1.2\ T_e$, which is also different from T_r. These crude estimates show that a small perturbation of the electron distribution from the Maxwellian one will affect the radiation temperature obtained from second harmonic emission, and that the value of T_r might be different from the temperature given by the thermal energy per unit volume $2\langle E\rangle/3n_e$. For a correct assessment of the electron temperature, a knowledge of the electron distribution in a wide range of electron energy is required. This goal is obtained by measuring the electron cyclotron emission in the full frequency range.

In order to illustrate the energy selection for the ESE, we consider the X-mode thermal emission normal to the magnetic field in the mid-plane for TFTR parameters[3], with $n_e = n_{e0}(1-$

$x^2/a^2)^{3.5}$, $T_e = T_{e0}(1-x^2/a^2)^{3.3}$, $n_{e0} = 0.9 \times 10^{20}$ m^{-3}, $T_{e0} = 11.5$ keV, and a magnetic field at the magnetic axis $B_a = 5.2$ T. Shown in Fig. 10 is $I_x(\omega)$ versus ω/ω_{ca}. The spectrum has maxima at $\omega/\omega_{ca} = 2.13, 3, 3.82, 4.52$, and minima at 2.43, 3.24, 4.15. For $\omega/\omega_{ca} > 3$, the emitted radiation is optically thin, and it is therefore affected by wall reflections (here, $R_f = 0.85$). Information on the spatial region of emission and the energy of the emitting electrons is obtained by plotting $G(\omega,x)$ versus x, for given values of ω. Shown in Fig. 11 is G versus x for $\omega/\omega_{ca} = 3, 3.75$, and 4, respectively. It appears that the predominant region of emission, namely the maximum of G, is a sensitive function of ω/ω_{ca}. For $\omega/\omega_{ca} = 3, 3.75$, and 4, we find $x_m \approx -9$, 0, and -20 cm, with half-widths $\Delta x \approx 7$, 16, and 15 cm, respectively. The energy of the emitting electrons $E_n = mc^2(n\omega_c/\omega - 1)$ is given by the first few harmonics with $n > n_0 = \omega/\omega_c(x)$. For $\omega/\omega_{ca} = 3$, $n_0 = 2.9$, hence $E_3 = 17$ keV. The next value of n, i.e. n = 4, gives a negligible contribution, since $E_4 = 193$ keV. For $\omega/\omega_{ca} = 3.75$, we obtain $E_4 = 34$ keV.

High frequency emission results from contributions of electrons with a wide spectrum of energies, and energy selection is obtained by varying the wave frequency. This is useful for investigating deviations from the Maxwellian distribution, as it occurs during rf heating and current drive. The resonant electron energies for the high-frequency spectrum in high-temperature plasmas are obtained in a similar way. For instance, for electrons radiating from a region where $T_e = 20$ keV, $n_e = 10^{20}$ m^{-3}, B = 5 T, and $\omega/\omega_c = 7$, the relevant contribution comes from the harmonics n = 8 and 9 (higher harmonics contribute to emission and absorption by less than 10 %). The energies of the radiating electrons are then 73 and 146 keV, respectively, namely, 3.6 T_e and 7.3 T_e. For $T_e = 30$ keV, the contribution of the 10th harmonic is no longer negligible: the corresponding resonant energy is 219 keV. The position x_m of maximum emission and the corresponding three first resonant energies $E_n(x_m)$ are shown in Fig. 12 (a and b, respectively), for $T_{e0} = 25$ keV, $n_{e0} = 2 \times 10^{20}$ m^{-3}, $\alpha_T = 2$, $R_f = 0.8$, y = 0. It appears that the full ESE spectrum is related to a wide range of plasma positions and energies, with well defined space and energy selection rules at every given frequency.

VI. Diagnosis of non-thermal distributions by ESE

The information content of ESE can be further enhanced by exploiting the Doppler effect, namely using oblique views with respect to the toroidal magnetic field. This allows the measurement of toroidal asymmetries[10] of the distribution function, namely, selection not only in energy, but also in $p_{\|}$, $p_{\perp}$. The absorption coefficient for oblique propagation and the resonant parallel and perpendicular momenta are presented in Appendix B.

In order to show some of the relevant features of oblique synchrotron emission, we investigate the angular dependence of $I_x(\omega)$. Shown in Fig. 13 is $I_x(\omega)$ versus ω/ω_{c0} for T_{e0} = 25 keV, $\alpha_T = 2$, $R_f = 0.8$, $y = 0$, and $\theta = 90°$, 65°, and 50°. It appears that $I_x(\omega)$ is nearly independent of θ for $\omega < \omega_b$. An angular dependence of $I_x(\omega)$ is found in the optically thin range of frequencies, namely, for $\omega > \omega_b$. This behavior is similar to that found by varying α_T and/or R_f. Oblique emission is particularly appropriate for diagnosing asymmetric non-thermal distributions. Isotropic and non-isotropic deviations from a Maxwellian at temperature T_e can occur during additional heating. Typical situations are the non-thermal deviations generated by rf current drive. The full analysis of this problem generally requires extensive Fokker-Planck computations, but a first useful step is the simple procedure of determining the presence of a deviation from the Maxwellian for given values of $v_{\|R}$ and $v_{\perp R}$. The bulk electron temperature T_b is assumed to be known. We consider the experimental spectrum at given angles $\theta_0 \neq 90°$. The maxima (minima) of emission occur at $\omega = \omega_i^*$ and we know that they are described by Eq. (3). A Maxwellian with bulk temperature T_b is used in Eq. (3) to compute $I(\omega_i^*)$. The computed value is compared with the experimental one: if the deviation from the Maxwellian is negligible, the two values of $I(\omega_i^*)$ should coincide. The deviation between the two values of $I(\omega_i^*)$, if any, reveals the presence of non-thermal electrons at $v_{\|R}(N_{\|})$ and $v_{\perp R}(N_{\|})$. Note that at frequencies $\omega = \omega_i^*$, the O-mode radiation is negligible compared to the X-mode and therefore there is no uncertainty on the polarization of the detected radiation at arbitrary $N_{\|}$.

The energy of the radiating electrons at $N_{\|} \neq 0$ is obtained from the relation $\gamma = \gamma_n = Y_n + N_{\|}v_{\|R}$. For instance, for $n_e = 10^{20}$ m^{-3}, B = 5 T, T_e = 30 keV, $\omega/\omega_c = 7$, and $N_{\|} = 0.34$, we obtain $\alpha = 0.27$ m^{-1}. If only the harmonics n = 8, 9, and 10 are retained, we obtain $\alpha = 0.25$

m^{-1}, and the corresponding energies are 113, 170 and 229 keV. For $\omega/\omega_c = 7.5$, the corresponding energies are 84, 138, and 193, respectively. For a given value of n, the parallel and perpendicular resonant velocities are given by $v_{\|R}$ and $v_{\perp R}$. For instance, for $T_e = 30$ keV, $N_\| = 0.5$, $\omega/\omega_c = 7.5$, and $n = 8$, we obtain $p_{\|R}/(mT_e)^{1/2} \approx 1.5$, and $p_{\perp R}/(mT_e)^{1/2} \approx 2.7$.

Asymmetric weakly non-Maxwellian electron distributions can occur on next-step tokamaks as a result of ion cyclotron fast wave current drive and/or a dc electric field E_{dc}. In this case, one expects a modest slide-away type parallel distribution and the emitted radiation is nearly thermal. Here, we briefly outline the procedure for investigating the weakly non-Maxwellian distribution using the maximum of the emitted spectrum at $N_\| \neq 0$.

The slide-away momentum distribution generated by small phase velocity traveling waves or by a dc electric field is represented by

$$f(v_\perp, v_\|) = f_M(v)\left[1 + g(v_\perp, v_\|)\right] ,$$

where $|g| < 1$, and f_M is the background Maxwellian distribution at temperature T_e assumed to be known. The function g is non-zero within a few thermal speeds, i.e., for $|p_\|| \leq 2(mT_e)^{1/2}$ and is assumed to be a slowly varying function of $v_\perp$, $v_\|$, compared to the variation of f_M. The local emission coefficient is given by

$$\eta(\omega, N_\|, x) = \frac{(\omega_p \mu / 4)^2}{\omega K_2(\mu) S}\left(\frac{\omega^2 T_e}{8\pi^3 c^2}\right) \sum_{n>n_0} Y_n^2 \int_{v_-}^{v_+} dv_\| \left[|P| J_n(\rho)\right]^2 (1+g)\exp(-\mu\gamma_n) .$$

Using the saddle point method of Ref. 2, we obtain

$$\eta(\omega, N_\|, x) = \sum_{n>n_0}\left[1 + g(v_{\|R}, v_{\perp R})\right]\eta_n(\omega, N_\|, x) ,$$

$$\text{where } \eta_n = \left(\frac{\omega^2 T_e}{8\pi^3 c^2}\right)\alpha_n(\omega, N_\|, x) ,$$

and α_n is given by Eq. (12), where $\alpha = \Sigma\alpha_n$. Now, for a given frequency we have found that only the first value of $n > n_0$ resonates with electrons with energy $E \leq 4T_e$, hence, $g \neq 0$ for the first relevant value of n, and we can write

$$\eta(\omega,N_{\parallel},x)=\left(\frac{\omega^2T_e}{8\pi^3c^2}\right)\left[\alpha_M+g(v_{\parallel R}^{(1)},v_{\perp R}^{(1)})\alpha_M^{(1)}\right] ,$$

where the subscript M refers to the Maxwellian distribution and the superscript (1) denotes the first relevant value of $n > n_0$. Using now Eq. (3) for oblique propagation, we can obtain the value of the parameter g from the experimental value of $I(\omega_i^*, N_{\parallel})$.

We here present a crude estimate of the enhancement of the emitted radiation caused by fast wave absorption and/or a dc electric field E_{dc}. Using Eq. (3) for $\theta_0 \neq 90°$, we obtain

$$I(\omega^*,\theta_0) = \frac{V(\omega^*,\theta_0)}{1-\left[\dfrac{dV/d\omega}{dV/d\omega+Vd\Phi/d\omega}\right]_{\omega^*}} ,$$

where

$$V(\omega,\theta_0)=\int_{-a}^{a}dx\,\eta(\omega,N_{\parallel},x)\exp[-\phi(\omega,N_{\parallel},x)]$$

$$=\frac{\omega^2}{8\pi^3c^2}\int_{-a}^{a}dx\,T_e(x)\left[\alpha_M(\omega,N_{\parallel},x)+g(v_{\parallel R}^{(1)},v_{\perp R}^{(1)})\alpha_M^{(1)}(\omega,N_{\parallel},x)\right]$$

$$\times\exp\left[-\phi_M(\omega,N_{\parallel},x)-g\phi_M^{(1)}(\omega,N_{\parallel},x)\right] ,$$

where $n_{e0} \rightarrow n_{e0}/|\sin\theta_0|$, and $g(v_{\parallel R}^{(1)},v_{\perp R}^{(1)})$ is computed at $x \approx 0$, where the source of radiation at $\omega = \omega^*$ is localized. We now consider $|g| \ll 1$ and approximate $I(\omega^*,\theta_0)$ by

$$I(\omega^*,\theta_0) \cong \frac{\omega^{*2}}{8\pi^3c^2}\int_{-a}^{a}dx\,T_e(x)\left[\alpha_M(\omega^*,N_{\parallel},x)+g\alpha_M^{(1)}(\omega^*,N_{\parallel},x)\right]\exp\left[-\phi_M(\omega^*,N_{\parallel},x)\right]$$

$$\times\left\{1-\left[\frac{dV_M/d\omega}{dV_M/d\omega+V_Md\Phi_M/d\omega}\right]_{\omega^*}\right\}^{-1} , \qquad (9)$$

where V_M and Φ_M are computed for a Maxwellian distribution. Equation (9) can be written as

$$\frac{I(\omega^*,\theta_0)-I_M(\omega^*,\theta_0)}{I_M(\omega^*,\theta_0)} = g(v_{\parallel R}^{(1)},v_{\perp R}^{(1)})\frac{I_M^{(1)}(\omega^*,\theta_0)}{I_M(\omega^*,\theta_0)} , \qquad (10)$$

where $v_{\parallel R}^{(1)},v_{\perp R}^{(1)}$ ar computed at $\omega = \omega^*$, $T_e = T_e(0)$, $N_{\parallel} = N_{\parallel}(0)$, and

$$I_M^{(1)}(\omega^*,\theta_0) = \frac{V_M^{(1)}(\omega^*,\theta_0)}{1-\left[\dfrac{dV_M/d\omega}{dV_M/d\omega + V_M d\Phi_M/d\omega}\right]_{\omega^*}} ,$$

$$V_M^{(1)}(\omega,\theta_0) = \frac{\omega^2}{8\pi^3 c^2}\int_{-a}^{a} dx\, T_e(x)\,\alpha_M^{(1)}(\omega,N_\parallel,x)\exp[-\phi_M(\omega,N_\parallel,x)] .$$

Since $I_M^{(1)}$, I_M can be computed using the Maxwellian at a given temperature profile, the experimental value of $I(\omega^*,\theta_0)$ allows the determination of $g(v_{\parallel R}^{(1)},v_{\perp R}^{(1)})$ on axis. In order to relate g with the fast-wave amplitude or the dc electric field, a 2D Fokker-Planck code is generally needed. An approximated derivation is obtained using the one-dimensional kinetic equation. Assuming $f(p_\perp,p_\parallel) = f(p_\perp)f(p_\parallel)$, the kinetic equation for fast-wave heating is

$$\frac{\partial f}{\partial t} = \frac{\partial}{\partial v_\parallel}\left(D_c\frac{\partial f}{\partial v_\parallel}\right) + \left(1+\frac{Z}{2}\right)\nu_0(T_e/m)^{3/2}\frac{\partial}{\partial v_\parallel}\left[\frac{1}{v_\parallel|v_\parallel|}\left(f_\parallel + \frac{T_e}{mv_\parallel}\frac{\partial f}{\partial v_\parallel}\right)\right] ,$$

$$\text{where } v_\parallel \approx p_\parallel/m \ , \quad Z = \sum_{\alpha\neq e} n_\alpha Z_\alpha^2/n_e \ , \quad \nu_0 = \Lambda\omega_p^4/2\pi n_e(T_e/m)^{3/2} \ ,$$

$$D_c = \frac{\pi e^2}{2m^2}\int_{-\infty}^{\infty} dn_\parallel |E_\parallel|^2\,\delta(\Omega - n_\parallel v_\parallel\Omega/c) .$$

$n_\parallel$ and $E_\parallel$ inside the integral refer to the fast wave with frequency Ω. The steady state solution is given by

$$f_\parallel(u_\parallel) = \frac{1}{(2\pi)^{1/2}}\exp\left[-\int_0^{u_\parallel} du_\parallel' \frac{u_\parallel'}{1+\mu(u_\parallel')/(2+Z)}\right] ,$$

where

$$u_\parallel = \frac{v_\parallel}{(T_e/m)^{1/2}} \ , \quad \mu(u_\parallel) = \frac{2|u_\parallel|^3 D_c(u_\parallel)}{\nu_0(T_e/m)} \ . \tag{11}$$

For $\mu(u_\parallel)/(2+Z) \ll 1$, we obtain

$$g(u_\perp,u_\parallel) = \frac{1}{2+Z}\int_0^{u_\parallel} du_\parallel' u_\parallel' \mu(u_\parallel') .$$

Note that for a given ω, the resonant energies of the relevant harmonics are too large apart and the derivation of Eq. (10) holds for $g \neq 0$ for $n = m$, with m different from the first relevant

value of $n > n_0$. For instance, we have shown that for $n_e = 10^{20}$ m^{-3}, B = 5 T, T_e = 30 keV, $\omega/\omega_c = 7.5$, and $N_{||} = 0.34$, the energies of the emitting electrons are 84, 138, and 193 keV, i.e., 2.8 T_e, 4.6 T_e, and 6.4 T_e. Equation (10) is then valid in a wide range of selective resonant energies.

The following order-of-magnitude estimate characterizes the minimum value of D_c for which a measurable deviation $\Delta I = I(\omega^*,\theta_0)-I_M(\omega^*,\theta_0)$ is found. Using Fig. 13, we find $I_M \approx 1200$ and the corresponding radiation temperature is $T_{rM} \approx 20$ keV. From Eq. (11), we obtain

$$g \approx \frac{2}{2+Z}\int_0^{u_{||}} du'_{||}u'^4_{||}\frac{D_c}{\nu_0(T_e/m)} \approx \frac{2}{2+Z}\frac{u_{||}^5}{5}\frac{D_c}{\nu_0(T_e/m)} .$$

Now, $I_{1M}/I_M \cong 1/2$, hence

$$\Delta T_r = T_r(\omega^*,\theta_0) - T_{rM}(\omega^*,\theta_0) \cong \tfrac{1}{2} g T_{rM} \cong \frac{1}{2+Z}\frac{u_{||}^5}{5}\frac{D_c}{\nu_0(T_e/m)}T_{rM} .$$

For $u_{||}^5/(2+Z) \cong 1$, and $\Delta T_r \cong 2$keV, we obtain $D_c/\nu_0(T_e/m) \cong 0.5$.

VII. Conclusions

A general scheme of plasma diagnostics for thermal and non-thermal plasmas, based on emission at arbitrary harmonics of the cyclotron frequency has been discussed. The motivation for developing a high frequency method of diagnostics is dictated by the limitations on ECE at the first few harmonics, imposed by high density and temperature regimes, and also by the very restrictive energy range of the emitting electrons near the resonance points. In the ESE method, the ray path is a straight line and cut-offs or refraction can be ignored. Furthermore, harmonic overlap is no longer a threat as it happens for emission near the second harmonic, and ESE is applicable to a plasma at arbitrary electron temperature. In the ESE method, the source of radiation is not highly localized in the ordinary space, but a kind of localization is found with a rather broad halfwidth of the spatial radiation line profile. However, the energy of the emitting electrons is now a sensitive function of the radiation frequency and any range of the electron energy can be selected by a small change of the wave frequency and/or the direction of emission.

The ESE method is based on a parametric characterization of the electron energy distribution in the phase space and the determination of the relevant parameters from the properties of the emitted spectrum. A general property is the relation between the effective reflection coefficient and the experimental values of the radiation intensity $I(\omega)$ for frequencies for which $dI(\omega)/d\omega = 0$, namely, at the maxima and minima of $I(\omega)$. This relation allows the determination of the adjustable parameters characterizing the electron distribution.

A special property of the emitted spectrum is the weak dependence of $I(\omega)$ on the temperature spatial profile for frequencies ω for which the plasma is optically thick. This special property is here used to determine the electron temperature on axis in the case of high temperature next-step tokamak plasmas, by best fitting the experimental spectra. The principal interest of the ESE scheme is plasma diagnostics in hot and dense tokamak plasmas, but a good deal of information on the validity and potential interest of the method can be obtained in present-day tokamaks at low and moderate temperature and density. In this case, the emission spectra display several maxima and minima, and it is therefore possible to characterize the electron distribution without any *ad hoc* choice of the reflection coefficient. This concept has been applied to the radiation spectra from TFTR during neutral beam heating to verify that the electron momentum distribution is a Maxwellian in all range of the electron energies from subthermal (second harmonic emission) to thermal and superthermal energies[3].

APPENDIX A. Emission and absorption coefficients for propagation normal to the magnetic field and arbitrary isotropic distributions

The absorption coefficient for propagation normal to the magnetic field is given by

$$\alpha_X(\omega) = (\omega / cN_X)\left[\varepsilon''_{22} + 2\varepsilon''_{12}(\varepsilon^0_{12}/\varepsilon^0_{11}) - \varepsilon''_{11}(\varepsilon^0_{12}/\varepsilon^0_{11})^2\right] , \qquad \omega > \omega_c$$

$$\alpha_O(\omega) = (\omega / cN_O)\varepsilon''_{33} , \qquad \omega \geq \omega_c$$

where $N_r = N_X$, N_O are the real indices of the X and O modes, respectively, in the cold plasma approximation, ε''_{ij} is the anti-Hermitian part of the relativistic plasma dielectric tensor, and ε^0_{ij} is the cold plasma tensor. For an isotropic electron momentum distribution f(p), following the derivation of Ref. 6, we obtain

$$\varepsilon''_{ij} = -\left(\frac{2\pi\omega_p}{\omega N_r}\right)^2 mc \sum_{n>n_0} \varepsilon''_{ij,n} Y_n^3 \left(\frac{\partial f}{\partial p}\right)_{\gamma=Y_n} .$$

The tensor $\varepsilon''_{ij,n}$ is given by

$$\varepsilon''_{11,n} = \frac{\pi}{2v} g_n J^2_{n+1/2}(v) ,$$

$$\varepsilon''_{12,n} = -i\varepsilon''_{11,n} + i\frac{\pi}{2n} g_n J_{n+1/2}(v) J_{n+3/2}(v) ,$$

$$\varepsilon''_{22,n} = \varepsilon''_{11,n} + \frac{\pi}{4n^2(n+2)} g_n \left\{ v(n+3)\left[J^2_{n+3/2}(v) - J^2_{n+1/2}(v)\right] - (2n^2 - n - 9) J_{n+1/2}(v) J_{n+3/2}(v) \right\}$$

$$\varepsilon''_{13,n} = \varepsilon''_{23,n} = 0 , \quad \varepsilon''_{33,n} = \frac{s^2}{2}\left[\varepsilon''_{11,n} - \left(\frac{\pi}{2v}\right) g_n J_{n-1/2}(v) J_{n+3/2}(v)\right] ,$$

$$v = N_r \frac{\omega}{\omega_c}\left(Y_n^2 - 1\right)^{1/2} , \quad s = \frac{v}{n} , \quad Y_n = \frac{n\omega_c}{\omega} ,$$

$$n_0 = \omega / \omega_c , \quad g_n = (2n+1)!!/2^n n! .$$

The emission coefficients are given by the same expressions of the absorption coefficients, with the substitution $\varepsilon''_{ij} \rightarrow G_{ij}$, where

$$G_{ij} = \left(\frac{2\pi\omega_p}{N_r}\right)^2 \frac{mc}{8\pi^3 c^2} \sum_{n>n_0} \varepsilon''_{ij,n} Y_n^2 [f(p)]_{\gamma=Y_n} .$$

The particular case of a Maxwellian distribution has been extensively discussed in the past[7-9]. The formulation presented here is valid for arbitrary frequencies $\omega > \omega_c$ and Larmor radius $\rho_L =$

$N_r(\omega/\omega_c)(p_\perp/mc)$. In fact, for propagation normal to the magnetic field, the energy of the resonant electrons is predominantly perpendicular to the magnetic field, $p \approx p_\perp$, hence, $p_\perp^2 \approx (mc)^2(\gamma^2-1) = (mc)^2(Y_n^2-1)$, and $\rho_L = N_r(\omega/\omega_c)(Y_n^2-1)^{1/2} = v$. Thus, for $v \ll 1$, one gets the familiar small Larmor radius formulas.

APPENDIX B. Emission coefficients and resonant velocities for oblique propagation

The absorption coefficient for arbitrary values of $N_\parallel$ is derived from the Poynting theorem

$$\alpha(\omega,x) = (\omega/c)\sum_{j\ell} A_j^* \varepsilon''_{j\ell} A_\ell \Big/ \left|\mathrm{Re}\left[\mathbf{E}^* \times (\mathbf{N}\times\mathbf{E})\right]\right| \qquad \text{(B1)}$$

where $\mathbf{E}$ is the wave electric field, $\mathbf{N} = (c/\omega)\mathbf{k}$ is the cold refractive index, and

$$A_1 = g\left[\varepsilon_{12}^0(\varepsilon_{33}^0 - N_\perp^2)\right] \ , \quad A_2 = g\left[(N_\perp N_\parallel)^2 - (\varepsilon_{11}^0 - N_\parallel^2)(\varepsilon_{33}^0 - N_\perp^2)\right] \ , \ A_3 = -gN_\perp N_\parallel \varepsilon_{12}^0 \ ,$$

The factor g is defined by the condition: $\Sigma_j A_j^* A_j = \mathbf{E}^*\cdot\mathbf{E}$. For a Maxwellian distribution, $\varepsilon''_{j\ell}$ can be cast in the following form

$$\varepsilon''_{j\ell} = \frac{\pi}{(1-N_\parallel^2)K_2(\mu)}\left(\frac{\omega_p\mu}{\omega N_\perp}\right)^2 \sum_{n>n_0} \varepsilon''_{j\ell,n} Y_n^2\left(Y_n^2 + N_\parallel^2 - 1\right)^{1/2} \exp\left(-\frac{\mu Y_n}{1-N_\parallel^2}\right) ,$$

where now $n_0 = (\omega/\omega_c)(1-N_\parallel^2)^{1/2}$.

For an arbitrary momentum distribution $f(p_\perp, p_\parallel)$, the absorption coefficient can be written as

$$\alpha(\omega, N_\parallel, x) = -\omega_p^2 \sum_{n>n_0} \int dp \left(\frac{D_n}{S}\right)\delta\left(\gamma - Y_n - \frac{N_\parallel p_\parallel}{mc}\right) L_n f(p_\perp, p_\parallel) \ ,$$

$$\text{where } \gamma = \left[1 + (p/mc)^2\right]^{1/2} \ ,$$

$$\gamma L_n = Y_n\left(\frac{\partial}{\partial p_\perp}\right) + \frac{N_\parallel p_\perp}{mc}\left(\frac{\partial}{\partial p_\parallel}\right) \ , \quad D_n = \frac{p_\perp}{8\omega}\left|\mathbf{E}\cdot\Pi_n\right|^2 \ ,$$

$$\Pi_{1n} = \frac{nJ_n(\rho)}{\rho} \ , \quad \Pi_{2n} = -iJ_n'(\rho) \ , \quad \Pi_{3n} = \frac{p_\parallel}{p_\perp} J_n(\rho) \ , \quad \rho = \frac{\omega}{\omega_c}\frac{N_\perp p_\perp}{mc} \ ,$$

and S is the magnitude of the Poynting vector. From Eq. (B1), we obtain

$$\alpha(\omega, N_{\parallel}, x) = -2\pi\omega_p^2 \sum_{n>n_0} \int_{v_-}^{v_+} dv_{\parallel} \left[\gamma \left(\frac{D_n}{S} \right) L_n f \right]_{v_{\perp}=v_n} , \qquad \text{(B2)}$$

where

$$v = \frac{p}{mc} \ , \quad v_n = \left(\gamma_n^2 - \gamma_{\parallel}^2 \right)^{1/2} \ , \quad \gamma_n = Y_n + N_{\parallel} v_{\parallel} \ , \quad \gamma_{\parallel} = \left(1 + v_{\parallel}^2 \right)^{1/2} \ ,$$

and

$$v_{\pm} = \frac{N_{\parallel} Y_n \pm \left(Y_n^2 + N_{\parallel}^2 - 1 \right)^{1/2}}{1 - N_{\parallel}^2} \ .$$

The emission coefficient is obtained from α with the substitution $L_n f \rightarrow -(\omega^2/8\pi^3 c^2) p_{\perp} f/m\gamma$. Note that for $f(p_{\perp}, p_{\parallel}) = f(p_{\perp}, -p_{\parallel})$, $\alpha(\omega, N_{\parallel}, x) = \alpha(\omega, -N_{\parallel}, x)$, and for $f(p_{\perp}, p_{\parallel}) \neq f(p_{\perp}, -p_{\parallel})$, $\alpha(\omega, N_{\parallel}, x) \neq \alpha(\omega, -N_{\parallel}, x)$, thus, differential emission of waves with equal and opposite values of $N_{\parallel}$ yields information on possible asymmetries of f.

We now use Eq. (B2) to derive a compact form of $\alpha(\omega, N_{\parallel}, x)$ for a Maxwellian distribution, and show the selective properties of emission in momentum space. For a Maxwellian distribution, Eq. (B2) becomes

$$\alpha(\omega, N_{\parallel}, x) = \frac{1}{\omega K_2(\mu) S} \left(\frac{\omega_p \mu}{4 N_{\perp}} \right)^2 \sum_{n>n_0} Y_n^2 \int_{v_-}^{v_+} dv_{\parallel} \left[|P| J_n(\rho) \right]^2 \exp(-\mu\gamma_n) , \qquad \text{(B3)}$$

where

$$|P| = \left| A_1 - i(\rho/n) \left[J_n'(\rho) / J_n(\rho) \right] A_2 + (N_{\perp} / Y_n) v_{\parallel} A_3 \right| \ ,$$

and $v_{\perp} = v_n$ in the integrand of Eq. (11). We only consider the X-mode. We note that for $\mu \gg 1$, $J_n^2(\rho)\exp(-\mu\gamma_n)$ has a sharp maximum at $v_{\parallel} = v_{\parallel R}$. This is then the predominant parallel velocity of the emitting (absorbing) electrons. The value of $v_{\parallel R}$ and the corresponding resonant perpendicular velocity $v_{\perp R}$ are given by

$$v_{\|R} = \left[|N_\|| Y_n - \left(Y_n^2 + N_\|^2 - 1 - Y_n^2 \Psi \right)^{1/2} \right] \Big/ \left(1 - N_\|^2 \right) ,$$

$$\Psi = \frac{1 + \left(Y_n^2 + N_\|^2 - 1 \right) \Big/ Y_n^2 - \left[\left(1 - N_\|^2 \right)^2 + 4\zeta Y_n^2 \left(Y_n^2 + N_\|^2 - 1 \right) \right]^{1/2} \Big/ Y_n^2}{2(1-\zeta)} ,$$

$$v_{\perp R} = Y_n \left[\Psi \Big/ \left(1 - N_\|^2 \right) \right]^{1/2} , \qquad \zeta = \left[N_\| \mu \omega_c \Big/ 2\omega \left(1 - N_\|^2 \right) \right]^2 .$$

These results are obtained for $N_\| > 0$. They hold for $N_\| < 0$ as well, but $v_{\|R}$ changes sign. $v_{\|R}$ can also be written as

$$v_{\|R} = \frac{N_\| Y_n}{1 - N_\|^2} \left\{ 1 - \left[\mu Y_n^2 \Big/ 2n \left(1 - N_\|^2 \right) \right] \Psi \Big/ (1 - \Psi)^2 \right\} .$$

The half-width $\Delta v_\|$ of the parallel resonance function is given by

$$(\Delta v_\|)^{-2} = \left[n \left(1 - N_\|^2 \right)^2 \Big/ Y_n^4 \Psi (1 - \Psi)^{1/2} \right] \left[\left(1 - N_\|^2 \right)^2 + 4\zeta Y_n^2 \left(Y_n^2 + N_\|^2 - 1 \right) \right]^{1/2} .$$

For $N_\| = 0$, $(\Delta v_\|)^{-2} \approx n_0^2/2$, i.e., $\Delta p_\| / (mT_e)^{1/2} \approx (2\mu / n_0^2)^{1/2}$. For $N_\| \to 1$, $(\Delta v_\|)^{-2} \approx \mu^2 / 2n$, i.e., $\Delta p_\| / (mT_e)^{1/2} \approx (2n/\mu)^{1/2} < 1$.

In terms of $v_{\|R}$, $\alpha(\omega, N_\|, x)$ can be written as

$$\alpha(\omega, N_\|, x) = \frac{1}{\omega K_2(\mu) S} \left[\frac{\omega_p \mu}{4 \left(1 - N_\|^2 \right)} \right]^2 \sum_{n > n_0} Y_n^2 \left(Y_n^2 + N_\|^2 - 1 \right)^{1/2} J_n^2(\rho_R) \exp\left[-\mu \left(N_\| v_{\|R} + Y_n \right) \right]$$

$$\times \left| A_1 - i \left(1 - \rho_R^2 / n^2 \right)^{1/2} A_2 + \left(N_\perp / Y_n \right) v_{\|R} A_3 \right| \frac{(-\pi\beta / 2t)^{1/2} (1 - t^2)^{3/2}}{\left[n^2 (1 + t^2) - \rho_R^2 \right]^{1/2}} , \tag{B4}$$

where

$$\rho_R = \delta (1 - t)^{1/2} , \quad t = \frac{2 v_{\|R} - (v_+ + v_-)}{v_+ - v_-} ,$$

$$\beta = \frac{\mu N_\|^2 \left(Y_n^2 + N_\|^2 - 1 \right)^{1/2}}{1 - N_\|^2} , \quad \delta = \frac{\omega N_\perp \left(Y_n^2 + N_\|^2 - 1 \right)^{1/2}}{\omega_c \left(1 - N_\|^2 \right)} .$$

See Ref. 2 for the details and accuracy of Eq. (B4).

REFERENCES

1 I. Fidone and G. Granata, Phys. Plasmas **1**, 1231 (1994).

2 I. Fidone, G. Granata and F. Geniet, Phys. Plasmas **1**, 1264 (1994).

3 I. Fidone, G. Giruzzi, and G. Taylor, Phys. Plasmas, submitted (Princeton Plasma Physics Laboratory Report PPPL-3111, June 1995).

4 K. Borrass, Fusion Technology **16**, 172 (1989).

5 K. Tomabechi, J.R. Gilleland, Yu.A. Sokolov, R. Toschi, and the ITER Team, Nucl. Fusion **31**, 1135 (1991).

6 G. Granata and I. Fidone, Journal of Plasma Phys. **45**, 361 (1991).

7 G. Bekefi, *Radiation Processes in Plasmas* (Wiley, New York, 1966).

8 B.A. Trubnikov, in *Reviews of Plasma Physics*, ed. by M.A. Leontovich (Consultant Bureau, New York, 1979), Vol. 7, p. 345.

9 W.E. Drummond and M.N. Rosenbluth, Phys. Fluids **3**, 45 (1960); ibid. **4**, 277 (1961); S. Tamor, Nucl. Fusion **18**, 229 (1978); M. Bornatici, R. Cano, O. De Barbieri, and F. Engelmann, Nucl. Fusion **23**, 1153 (1983); D.B. Batchelor, R.C. Goldfinger, and N. Weitzner, Phys. Fluids **27**, 2385 (1985).

10 G. Giruzzi, I. Fidone, and M.J. Marchã, Nucl. Fusion **31**, 517 (1991).

FIGURE CAPTIONS

Fig. 1 - (a) $T_r(f)$ vs $f = \omega/2\pi$, for the O-mode, $T_{e0} = 20$ keV, $\alpha_T = 1$, $n_{e0} = 10^{20}$ m^{-3} (full thin), and $n_{e0} = 2 \times 10^{20}$ m^{-3} (dotted). The full thick curve is $T_e(x_c)$ versus $f = f_c(x_c)$. (b) As in Fig. 1(a), for $\alpha_T = 3$.

Fig. 2 - $T_r(f)$ vs f, for the O-mode, $T_{e0} = 25$ keV, $\alpha_T = 1$, $n_{e0} = 10^{20}$ m^{-3} (full thin), $n_{e0} = 2 \times 10^{20}$ m^{-3} (dotted thin), and $n_{e0} = 2 \times 10^{20}$ m^{-3}, $\alpha_T = 3$ (dashed thin). The full thick curves represent the corresponding $T_e(x_c)$ versus $f = f_c(x_c)$.

Fig. 3 - Ray trajectories for $n_{e0} = 2 \times 10^{20}$ m^{-3}, f = 130 GHz, and several values of y.

Fig. 4 - $T_r(f)$ vs f, for the X-mode, $T_{e0} = 15$ keV, $\alpha_T = 1$, and $n_{e0} = 10^{20}$ m^{-3}.

Fig. 5 - $I_x(\omega)$ (a), $I_o(\omega)$ (b), and $t_{x,o}(\omega)$ (c) vs ω/ω_{c0}, for $T_{e0} = 20$ and 30 keV, $\alpha_T = 2$, $n_{e0} = 2 \times 10^{20}$ m^{-3}, $R_f = 0.8$ (full) and $R_f = 0$ (dotted).

Fig. 6 - $I_x(\omega)$ vs ω/ω_{c0}, for $T_{e0} = 25$ keV, $n_{e0} = 2 \times 10^{20}$ m^{-3}, $\alpha_T = 1.5$ (full), $\alpha_T = 3$ (dotted), and $R_f = 0$, 0.8, 1.

Fig. 7 - $G_x(\omega,x)$ vs x, for $T_{e0} = 25$ keV, $n_{e0} = 2 \times 10^{20}$ m^{-3}, $\alpha_T = 2$, and $\omega/\omega_{c0} = 4$, 5,6,7,and 10.

Fig. 8 - $T_{r1}(\omega)$ vs ω/ω_{c0}, for $T_{e0} = 25$ keV, $n_{e0} = 2 \times 10^{20}$ m^{-3}, $\alpha_T = 1.5$ (full), $\alpha_T = 3$ (dotted), and $R_f = 1$.

Fig. 9 - $I_x(\omega)$ (a) and $t_x(\omega)$ (b) vs ω/ω_{c0}, for $T_{e0} = 25$ keV, $n_{e0} = 2 \times 10^{20}$ m^{-3}, $\alpha_T = 2$, $R_f = 0.8$, and several values of y.

Fig.10 - $I_x(\omega)$ vs ω/ω_{ca}, for TFTR parameters.

Fig.11 - $G_x(\omega,x)$ vs x, for $\omega/\omega_{ca} = 3$, 3.75, and 4, and the parameters of Fig. 10.

Fig.12 - $T_{e0} = 25$ keV, $n_{e0} = 2 \times 10^{20}$ m^{-3}, $\alpha_T = 2$, $R_f = 0.8$, y = 0. (a) x_m and I_x vs ω/ω_{c0}. (b) $E_n(x_m)$ vs ω/ω_{c0}.

Fig.13 - $I_x(\omega)$ vs ω/ω_{c0}, for $T_{e0} = 25$ keV, $n_{e0} = 2 \times 10^{20}$ m^{-3}, $\alpha_T = 2$, $R_f = 0.8$, y = 0, and $\theta_0 = 90°$, 65°, and 50°.

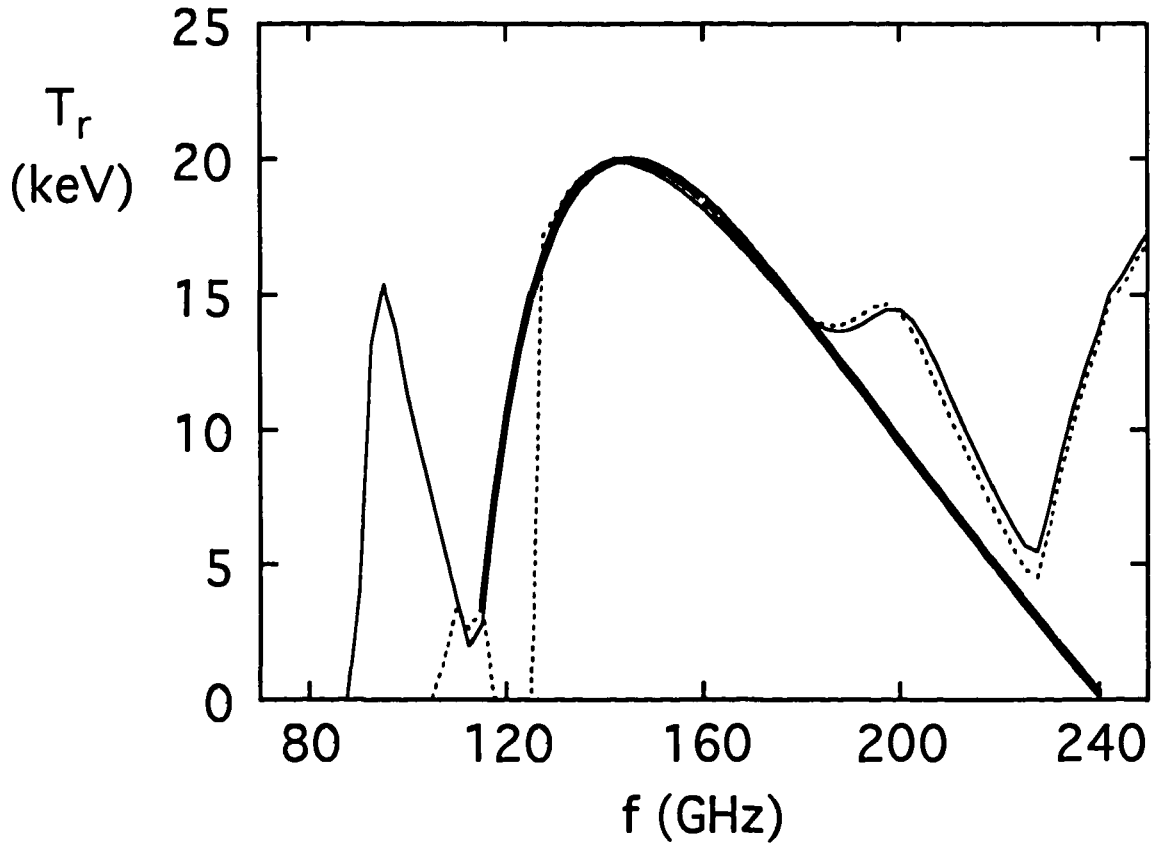

Fig. 1(a)

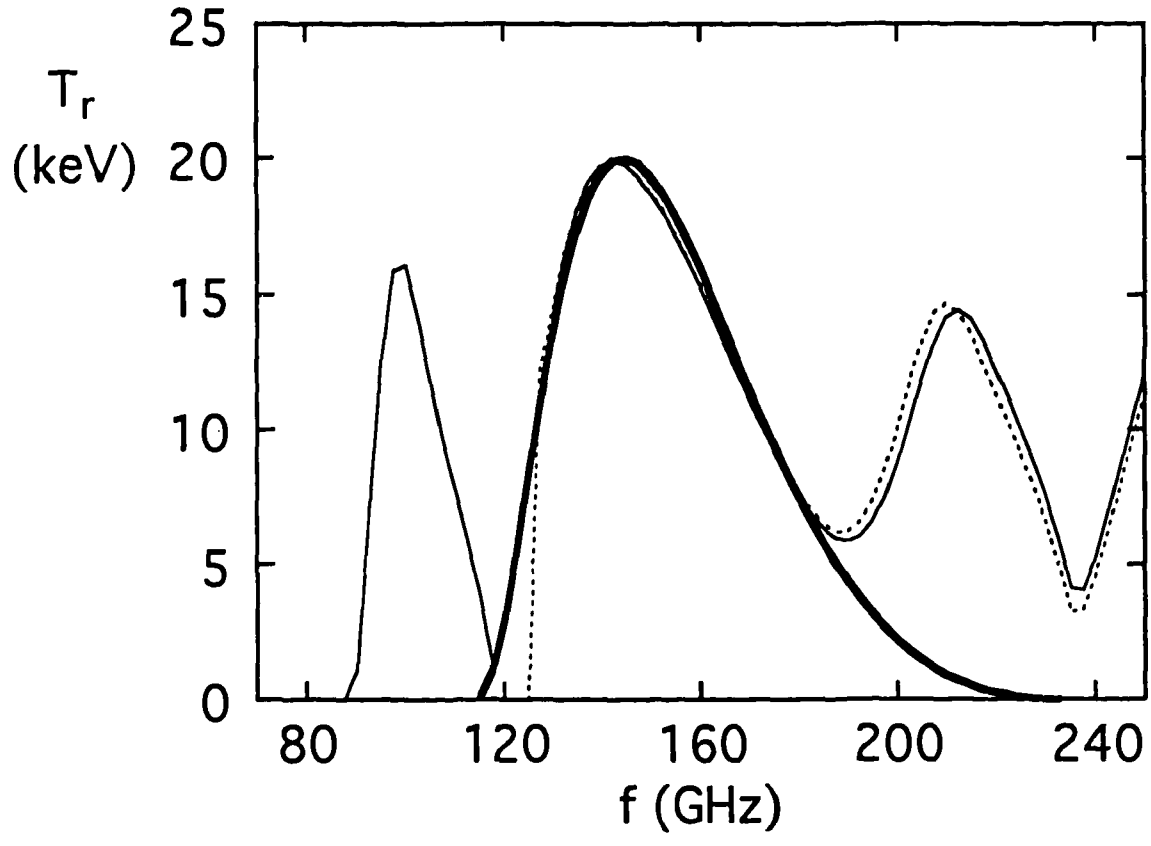

Fig. 1(b)

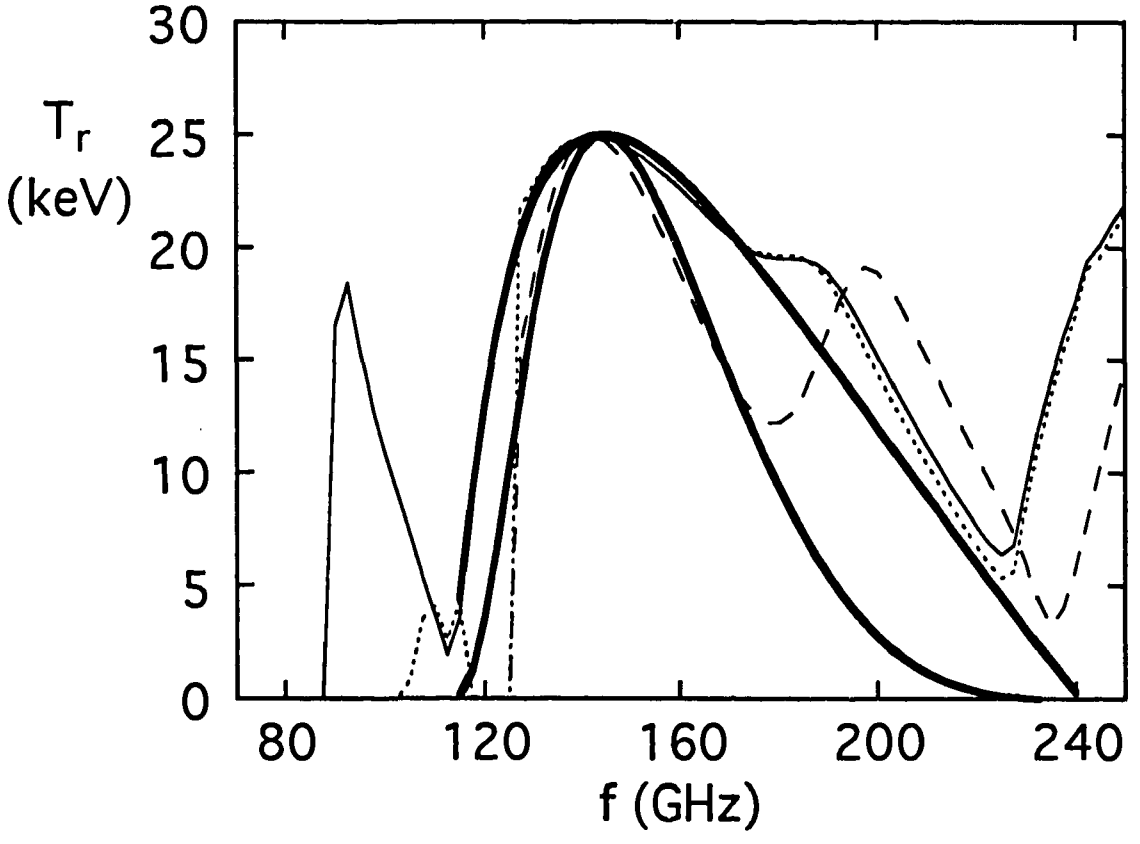

Fig. 2

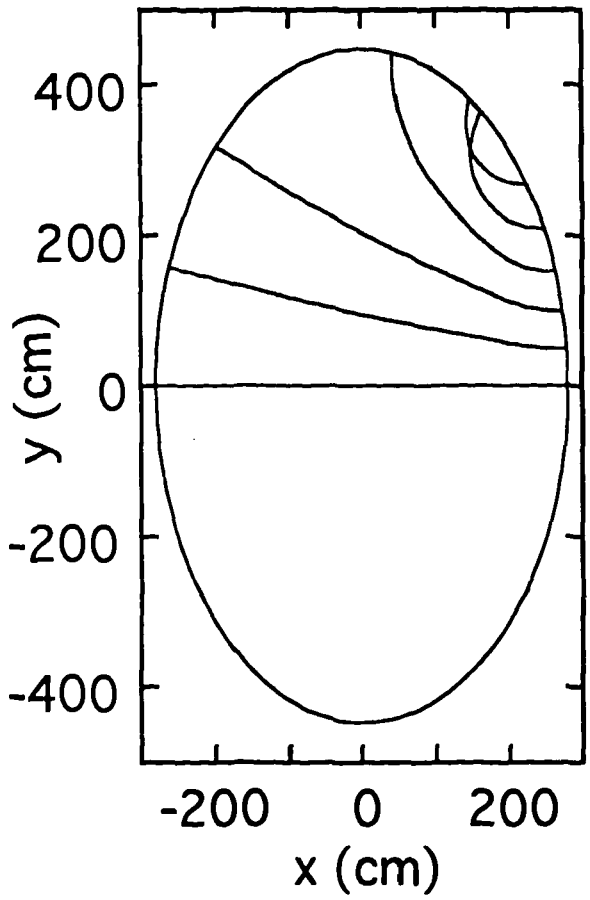

Fig. 3

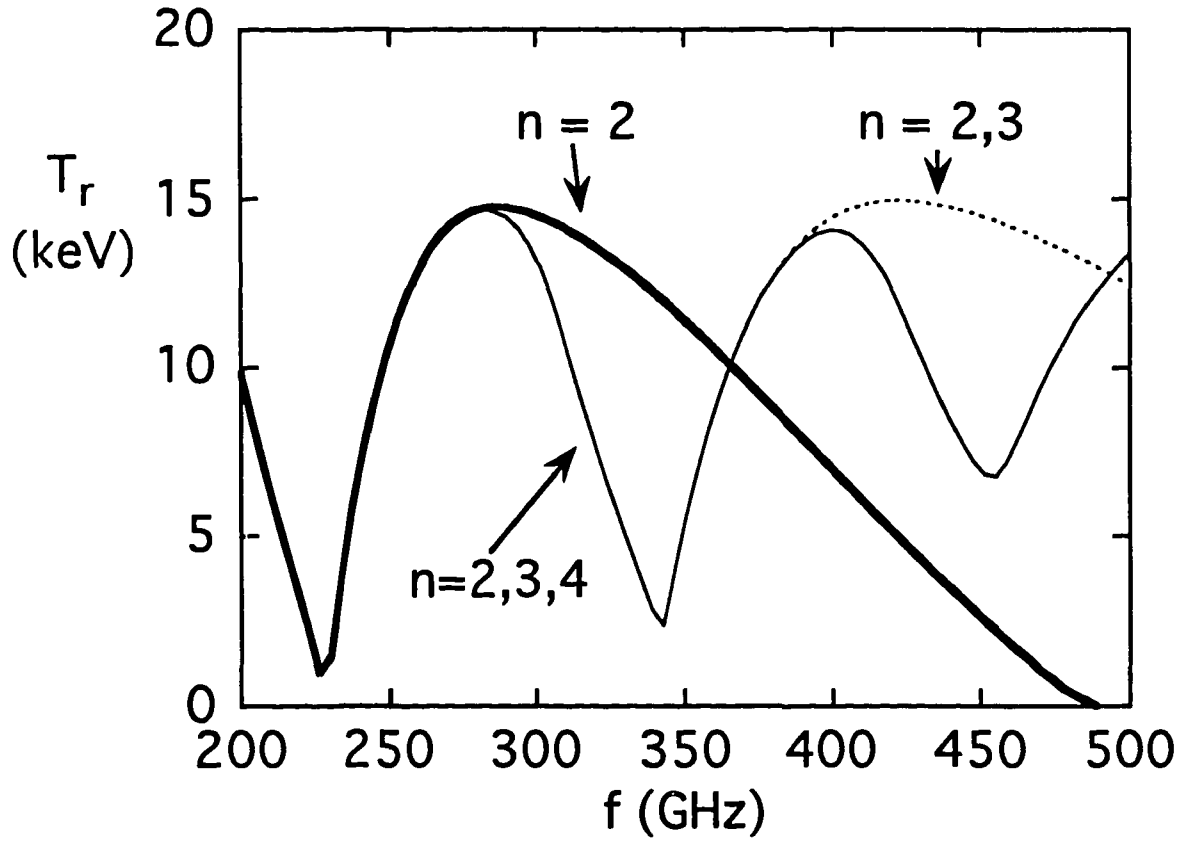

Fig. 4

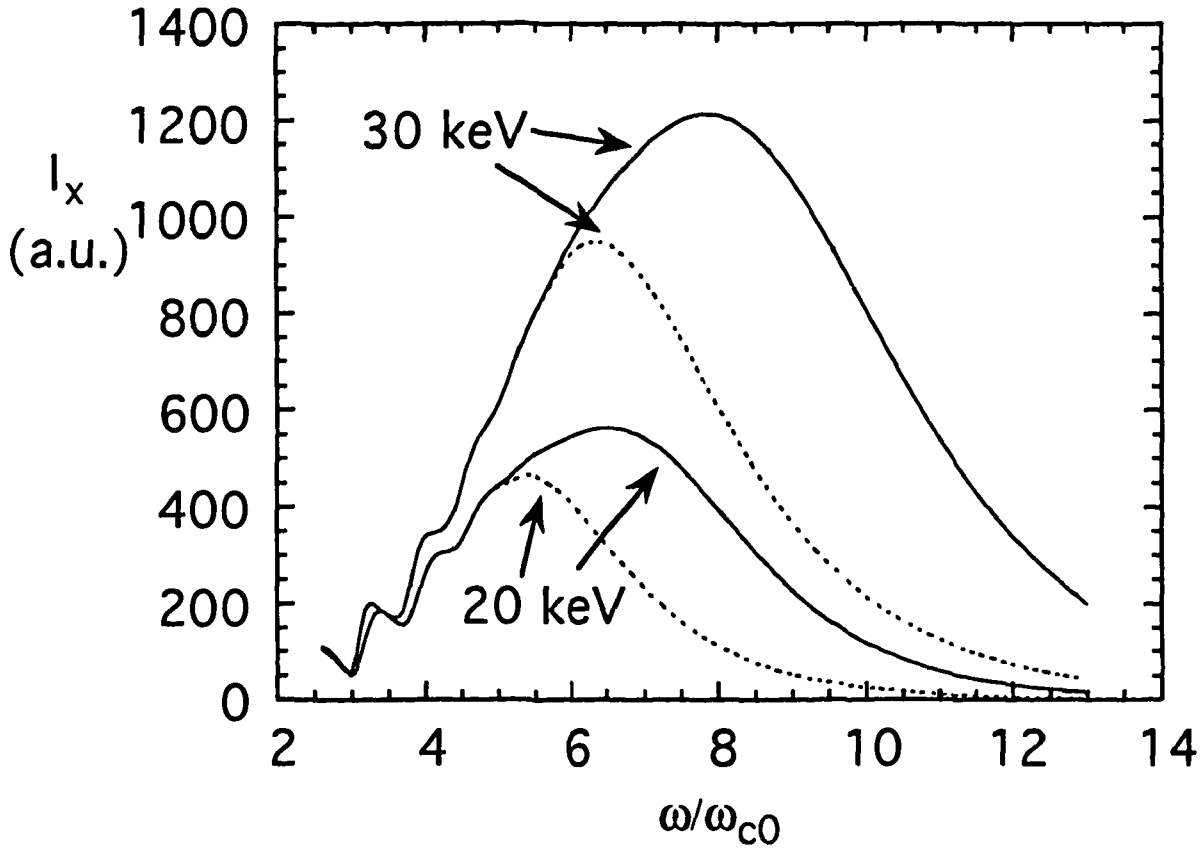
1400
1200
1000
800
600
400
200
0
I_x
(a.u.)
30 keV
20 keV
2
4
6
8
10
12
14
ω/ω_{c0}

Fig. 5(a)

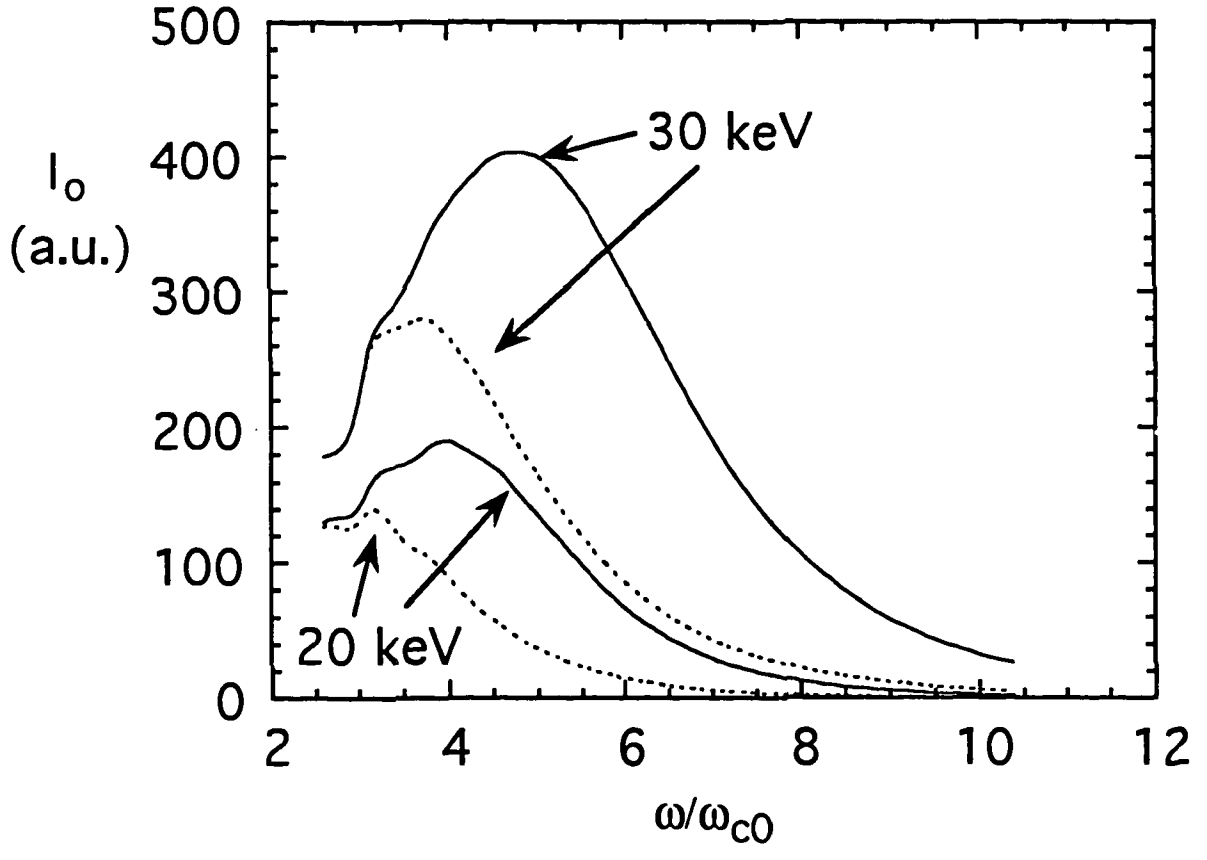
500
400
300
200
100
0
I_o
(a.u.)
30 keV
20 keV
2
4
6
8
10
12
ω/ω_{c0}

Fig. 5(b)

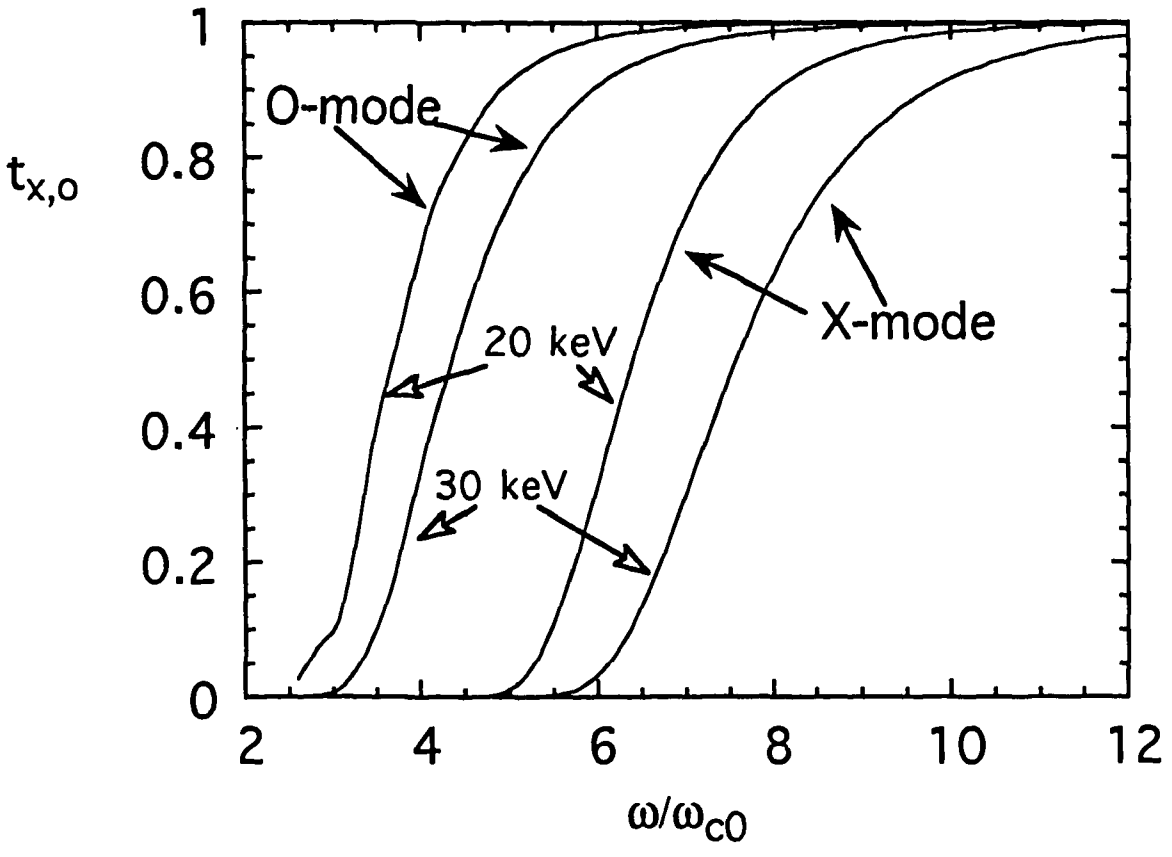
1
0.8
0.6
0.4
0.2
0
$t_{x,o}$
O-mode
X-mode
20 keV
30 keV
2
4
6
8
10
12
ω/ω_{c0}

Fig. 5(c)

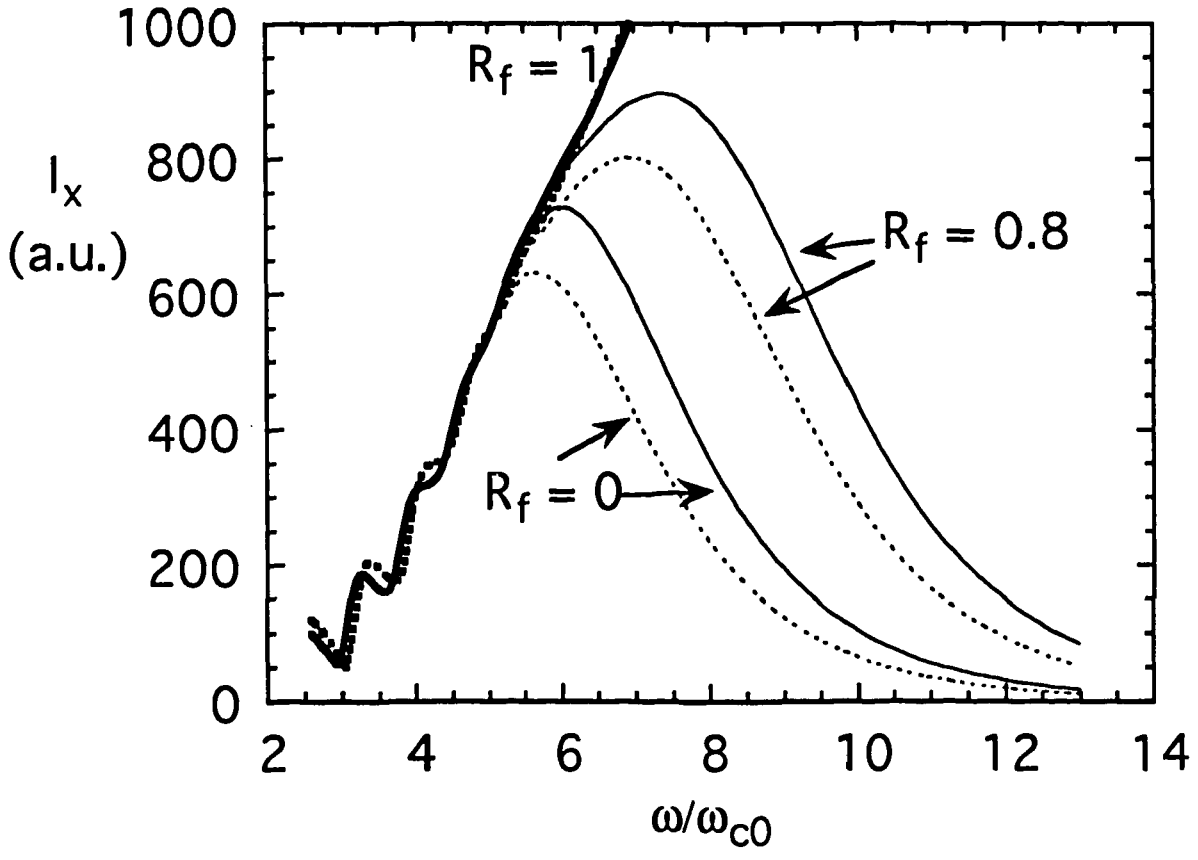
1000
800
600
400
200
0
I_x
(a.u.)
R_f = 1
R_f = 0.8
R_f = 0
2
4
6
8
10
12
14
ω/ω_{c0}

Fig. 6

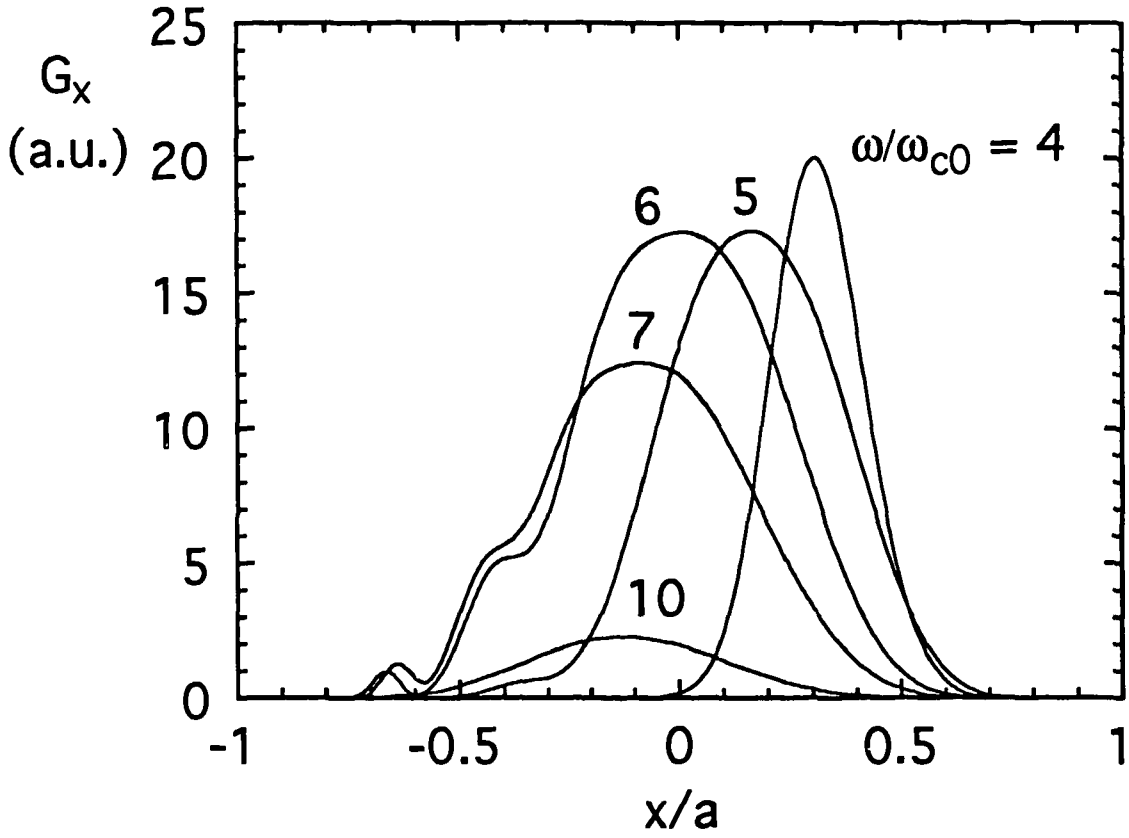

Fig. 7

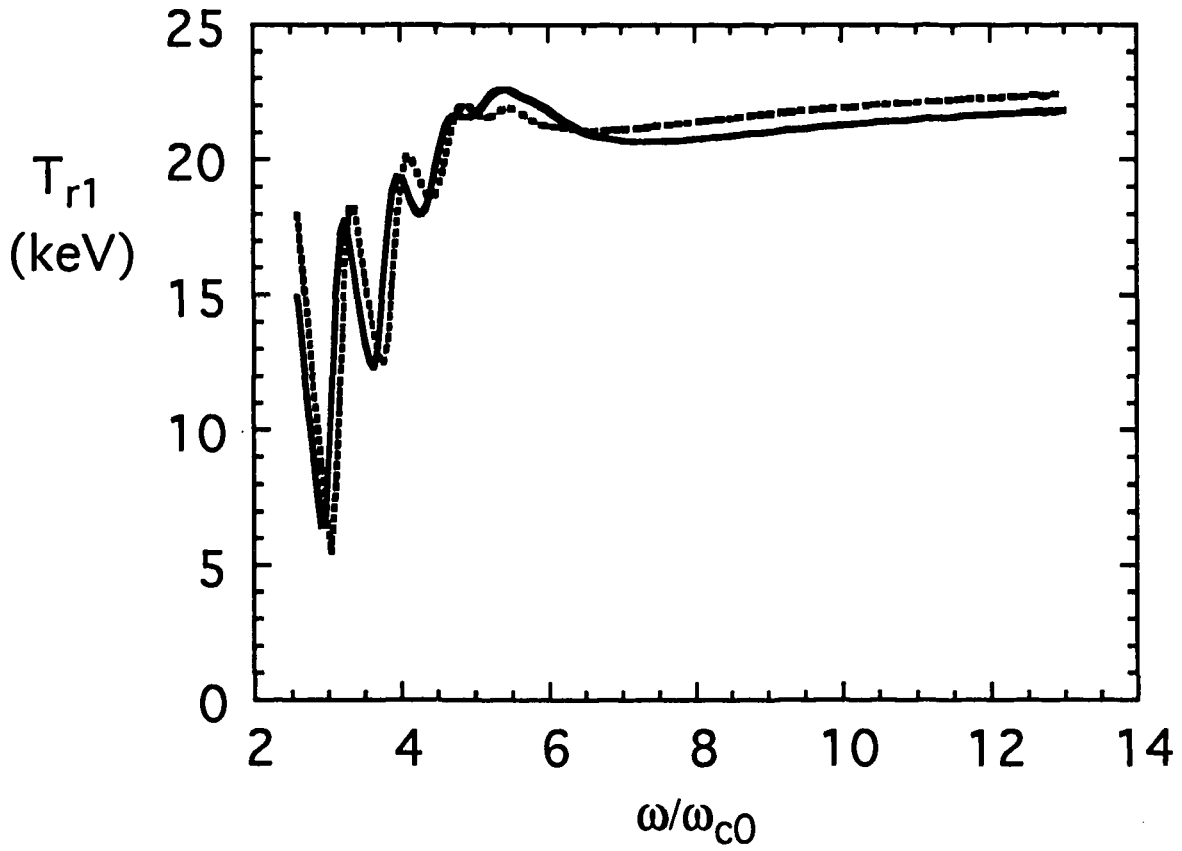

Fig. 8

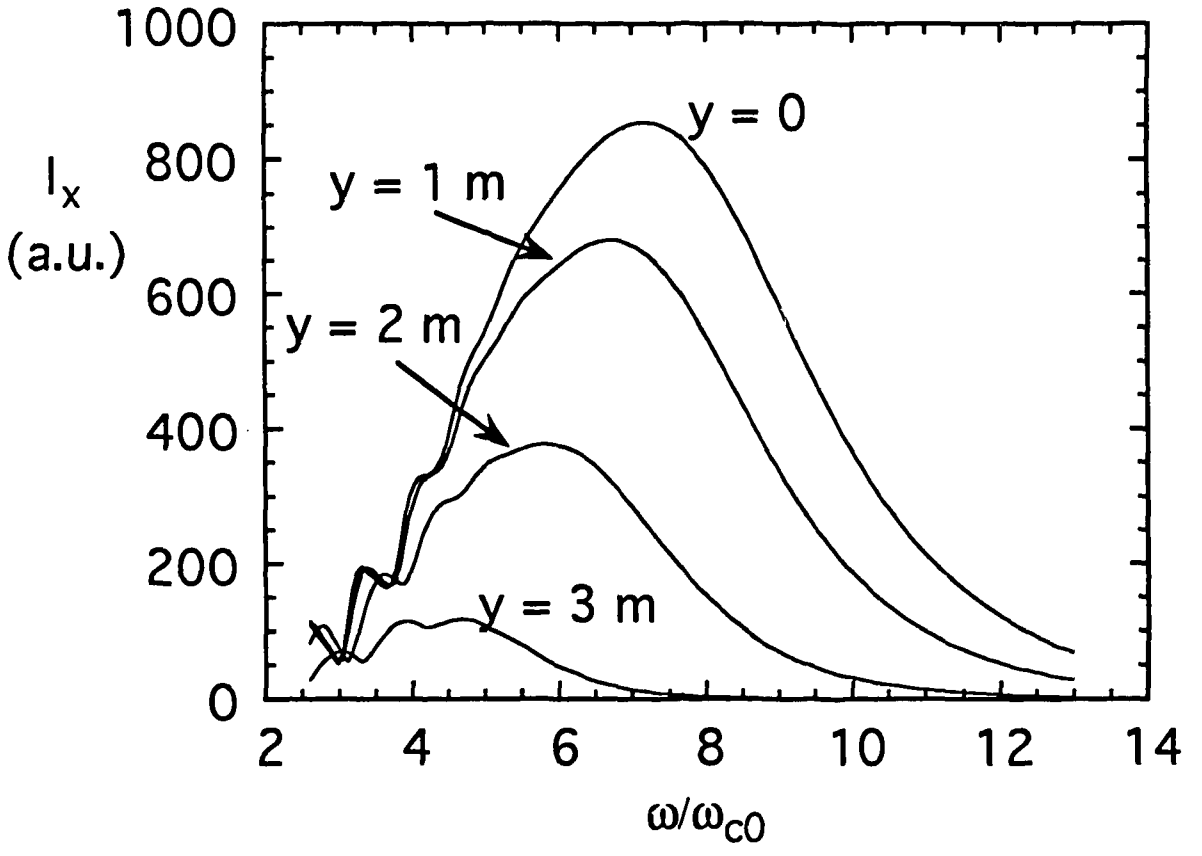
1000
800
600
400
200
0
I_x
(a.u.)
y = 0
y = 1 m
y = 2 m
y = 3 m
2
4
6
8
10
12
14
ω/ω_{c0}

Fig. 9(a)

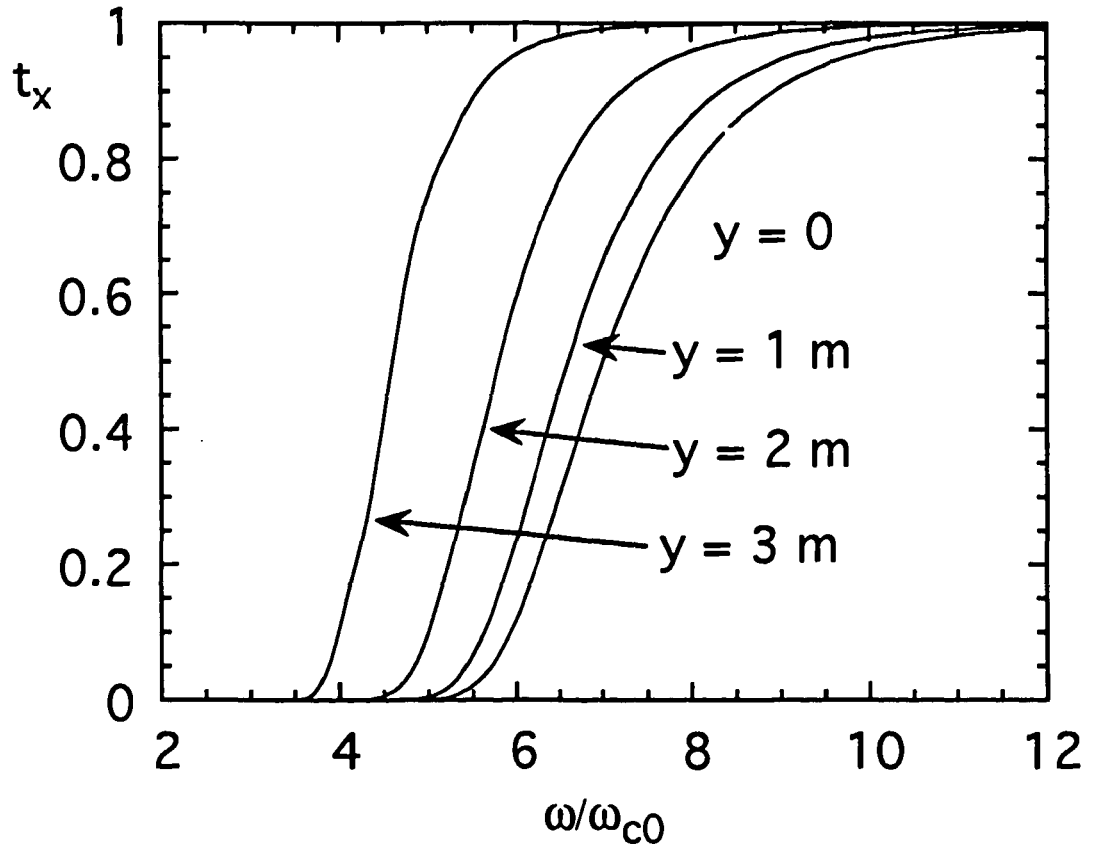

Fig. 9(b)

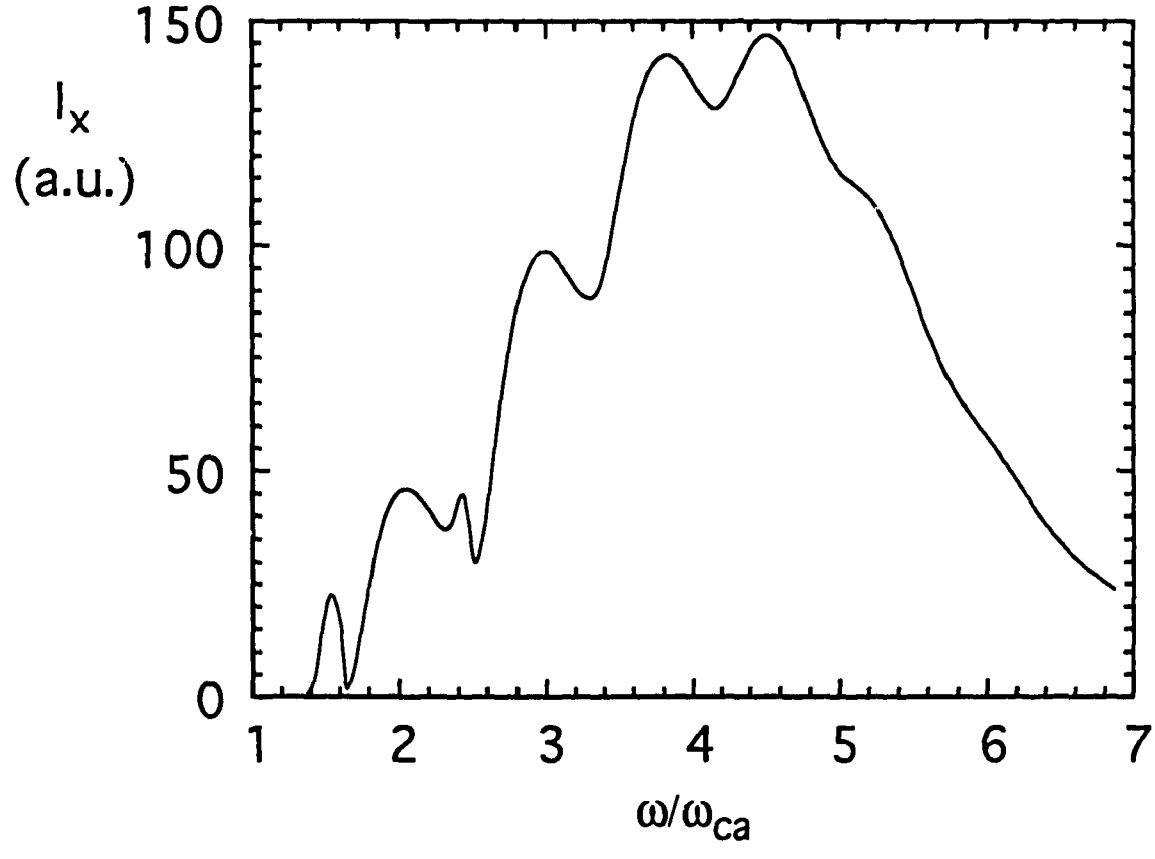

Fig. 10

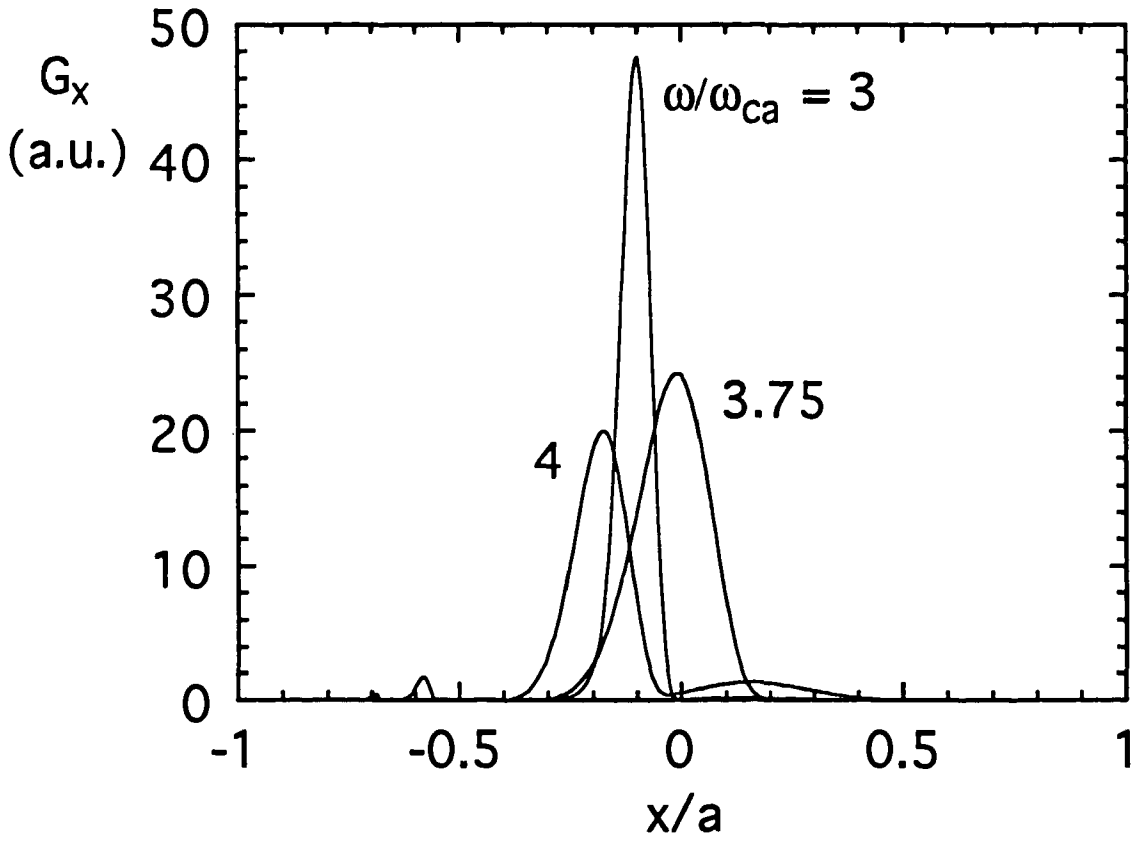

Fig. 11

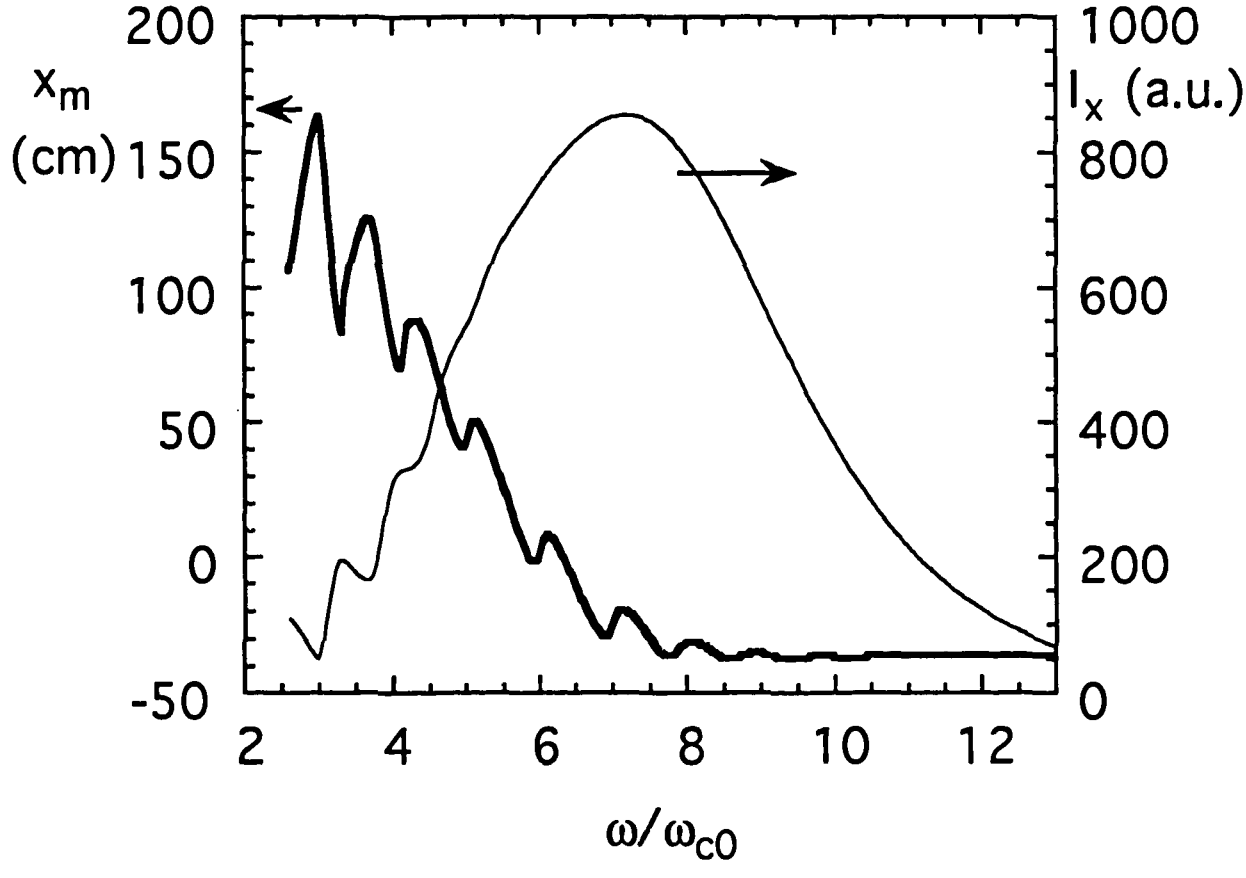
200
150
100
50
0
-50
x_m
(cm)
1000
800
600
400
200
0
I_x (a.u.)
2
4
6
8
10
12
ω/ω_{c0}

Fig. 12(a)

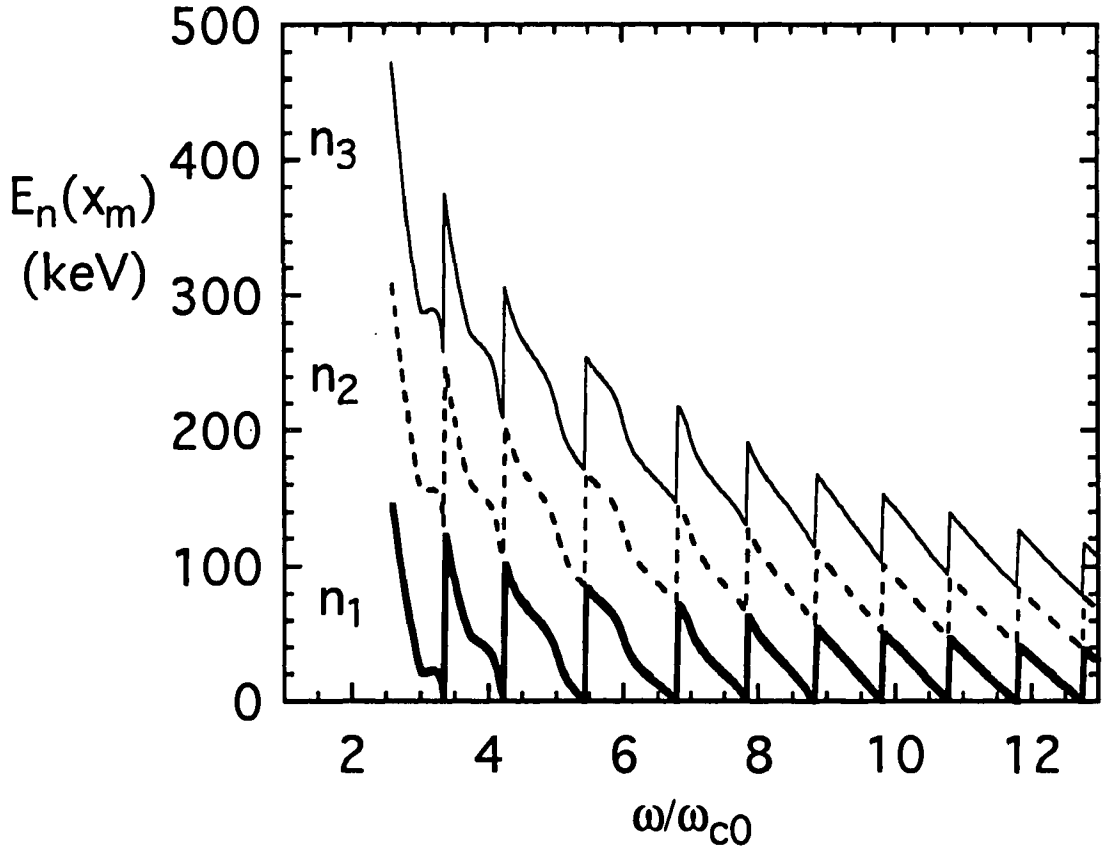

Fig. 12(b)

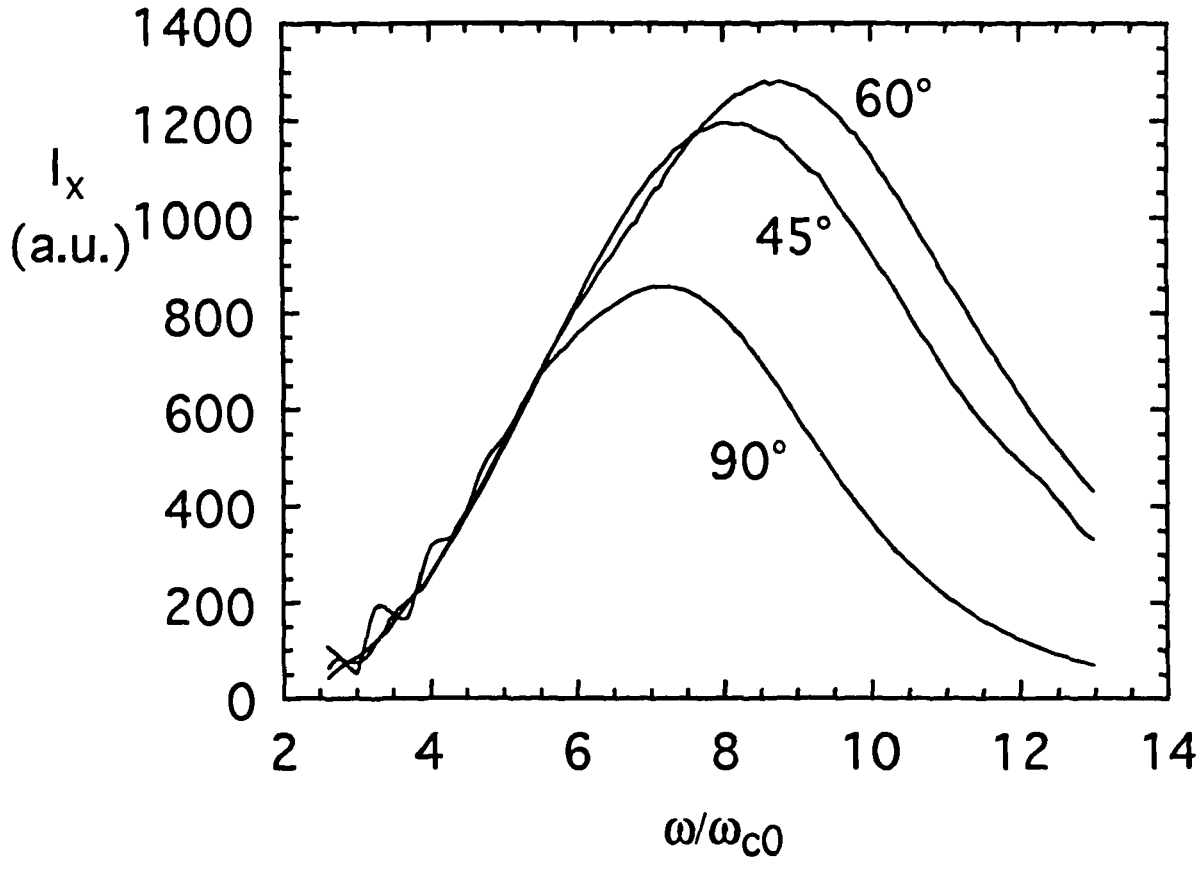
1400
1200
1000
800
600
400
200
0
I_x
(a.u.)
60°
45°
90°
2
4
6
8
10
12
14
ω/ω_{c0}

Fig. 13